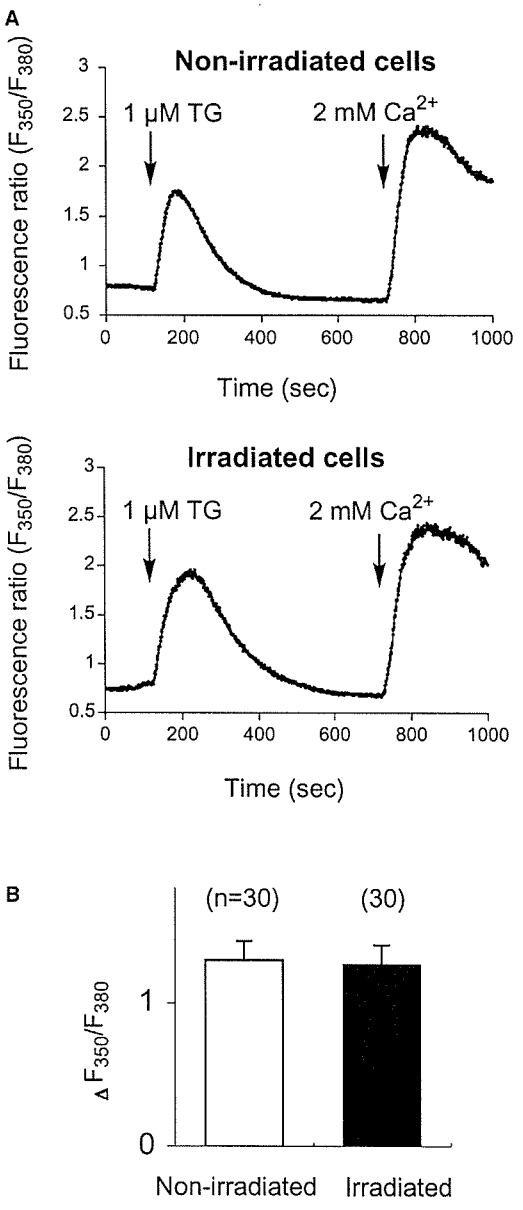

Figure 4. The Effect of $MGIP_3$/PM-Mediated smCALI on Thapsigargin-Induced Capacitative Calcium Entry in DT40 Cells

(A) Intracellular Ca^{2+} release and Ca^{2+} influx were measured in TG-stimulated irradiated and nonirradiated cells. After washing of the cells with Ca^{2+}-free solution, 1 μM TG was used to deplete the Ca^{2+} store, followed by addition of 2 mM Ca^{2+}.

(B) Increase of fluorescence ratio induced by addition of 2 mM Ca^{2+} after TG treatment of irradiated and nonirradiated cells. No significant difference was found between irradiated and nonirradiated cells ($p > 0.86$). The number of analyzed cells is indicated on top of each column. These data were acquired in three independent experiments. Results are the mean ± SEM.

this method is powerful, toxicity and nonspecific damage [27] can be problematic. In our smCALI strategy, we showed that there is no apparent nonspecific damage to IP_3R, presumably due to the catalytic nature of the inactivation and high efficiency. We demonstrated that intracellular Ca^{2+} dynamics can be modified by smCALI of IP_3R under physiological conditions. Since IP_3R is an important regulator of intracellular Ca^{2+} dynamics, spatiotemporally specific inactivation of IP_3R by smCALI using $MGIP_3$/PM may provide a useful method for clarifying the complex Ca^{2+} signaling mechanisms in intact living cells. smCALI should also be applicable to targets other than IP_3R, if appropriate malachite green-conjugated ligands are synthesized.

Experimental Procedures

Synthesis of $MGIP_3$/PM

$MGIP_3$ was synthesized as reported previously [8]. To synthesize $MGIP_3$/PM, $MGIP_3$ (1.0 eq.) was mixed vigorously with CH_3CN and *N, N*-diisopropylethylamine (DIEA) (2.0 eq.). The mixture was then dried under vacuum. This procedure was repeated at least three times until a homogenous solution was obtained after adding CH_3CN/DIEA. After a final round of drying, the green solid was suspended in CH_3CN and DIEA (5.0 eq.). Bromomethyl propionate (5.0 eq.) [28] was added to this solution. The mixture was stirred for 24 hr, then further bromomethyl propionate (2.5 eq.) and DIEA (2.5 eq.) were added and the reaction was continued for another 24 hr. The solvent and excess reagents were evaporated under vacuum. The remaining mixture was purified by C_{18} reversed-phase HPLC. ^{1}H-NMR (CD_3OD): δ1.02 (m, 15H), 1.80 (m, 2H), 1.93 (br, 2H), 2.32 (m, 10H), 3.30~5.50 (m, 10H), 3.60 (s, 12H), 5.61 (br, 10H), 7.30 (m, 2H), 7.58 (m, 4H), 7.78 (m, 6H). 1L-$MGIP_3$/PM was also synthesized in the same manner.

Cell Culture

DT40 chicken B lymphoma cells were cultured in RPMI1640 supplemented with 10% fetal calf serum (FCS), 1% chicken serum, penicillin (100 U/ml), streptomycin (100 U/ml), and 2 mM glutamine. In some experiments, genetically engineered DT40 cells that express only type 2 IP_3R or that lack all three type of IP_3R were used [11, 12].

Ca^{2+} Imaging

Cells were attached to poly-L-lysine and collagen-coated coverslips and loaded with 1 μM Fura-2AM (Molecular Probes) for 30 min in a physiological salt solution (PSS: 150 mM NaCl, 4 mM KCl, 2 mM $CaCl_2$, 1 mM $MgCl_2$, 5 mM HEPES, 5.6 mM glucose, pH 7.4) containing 0.1% bovine serum albumin (BSA). An Olympus IX71 inverted microscope, equipped with a cooled CCD camera (Photometrics) and a polychromatic illumination system (T.I.L.L. Photonics) was used to capture the fluorescence images generated by alternate excitations at 350 and 380 nm every 1 or 10 s. Intracellular Ca^{2+} concentration was measured as the ratio of the fluorescence intensity between the pair of frames (F_{350}/F_{380}). The test compounds were predissolved in PSS (containing 0.1% DMSO).

Laser Irradiation for smCALI

A nitrogen-driven pulsed dye laser (wavelength 635 nm, pulse width <4 ns, and pulse energy ~30 μJ at 20 Hz; Laser Science Inc.;VSL-337ND-S and DUO-220) was spatially filtered using a pair of objective lenses. A circular beam with a required spot size was introduced into a water-immersion objective (60×, NA 0.90, Olympus) attached to the inverted fluorescence microscope. The laser beam was focused onto a single DT40 cell. The diameters of the laser spot and a single DT40 cell were 20 and ~15 μm, respectively. The laser pulse energy at the focal plane was ~7 μJ. Laser irradiation was carried out as follows. The probe was added to the extracellular solution of Fura-2-loaded DT40 cells, and after 60 min, the excess ester was washed away with PSS. After ≥30 min, several cells were successively irradiated for 60 s. For the analysis of nonirradiated

cells surrounding irradiated cells, we randomly selected cells within a frame.

Statistical Analyses

Statistical analysis was performed using Student's unpaired t-test.

Acknowledgments

This work was supported in part by the Ministry of Education, Culture, Sports, Science, and Technology of Japan (grants 11794026, 12470475, and 12557217 to T.N., 13558078, 14045210, and 15681012 to K.K.), by the Mitsubishi Foundation, and by the Research Foundation for Opt-Science and Technology.

Received: January 18, 2004
Revised: May 6, 2004
Accepted: May 11, 2004
Published: August 20, 2004

References

1. Schmucker, D., Su, A.L., Beermann, A., Jäckle, H., and Jay, D.G. (1994). Chromophore-assisted laser inactivation of patched protein switches cell fate in the larval visual-system of *Drosophila*. Proc. Natl. Acad. Sci. USA *91*, 2664–2668.
2. Vernos, I., Raats, J., Hirano, T., Heasman, J., Karsenti, E., and Wylie, C. (1995). Xklp1, a chromosomal *Xenopus* kinesin-like protein essential for spindle organization and chromosome positioning. Cell *81*, 117–127.
3. Kiselyov, K., Xu, X., Mozhayeva, G., Kuo, T., Pessah, I., Mignery, G., Zhu, X., Birnbaumer, L., and Muallem, S. (1998). Functional interaction between $InsP_3$ receptors and store-operated Htrp3 channels. Nature *396*, 478–482.
4. Jay, D.G. (1988). Selective destruction of protein function by chromophore-assisted laser inactivation. Proc. Natl. Acad. Sci. USA *85*, 5454–5458.
5. Jay, D.G., and Sakurai, T. (1999). Chromophore-assisted laser inactivation (CALI) to elucidate cellular mechanisms of cancer. Biochim. Biophys. Acta *1424*, M39–M48.
6. Berridge, M.J. (1993). Inositol trisphosphate and calcium signaling. Nature *361*, 315–325.
7. Berridge, M.J., Bootman, M.D., and Roderick, H.L. (2003). Calcium signalling: dynamics, homeostasis and remodelling. Nat. Rev. Mol. Cell Biol. *4*, 517–529.
8. Inoue, T., Kikuchi, K., Hirose, K., Iino, M., and Nagano, T. (1999). Synthesis and evaluation of 1-position-modified inositol 1,4,5-trisphosphate analogs. Bioorg. Med. Chem. Lett. *9*, 1697–1702.
9. Inoue, T., Kikuchi, K., Hirose, K., Iino, M., and Nagano, T. (2001). Small molecule-based laser inactivation of inositol 1,4,5-trisphosphate receptor. Chem. Biol. *8*, 9–15.
10. Inoue, T., Kikuchi, K., Hirose, K., Iino, M., and Nagano, T. (2003). Spatiotemporal laser inactivation of inositol 1,4,5-trisphosphate receptors using synthetic small-molecule probes. Chem. Biol. *10*, 503–509.
11. Sugawara, H., Kurosaki, M., Takata, M., and Kurosaki, T. (1997). Genetic evidence for involvement of type 1, type 2 and type 3 inositol 1,4,5-trisphosphate receptors in signal transduction through the B-cell antigen receptor. EMBO J. *16*, 3078–3088.
12. Miyakawa, T., Maeda, A., Yamazawa, T., Hirose, K., Kurosaki, T., and Iino, M. (1999). Encoding of Ca^{2+} signals by differential expression of IP_3 receptor subtypes. EMBO J. *18*, 1303–1308.
13. Prestwich, G.D., Marecek, J.F., Mourey, R.J., Theibert, A.B., Ferris, C.D., Danoff, S.K., and Snyder, S.H. (1991). Tethered IP_3. Synthesis and biochemical applications of the 1-*O*-(3-aminopropyl) ester of inositol 1,4,5-trisphosphate. J. Am. Chem. Soc. *113*, 1822–1825.
14. Venkatachalam, K., van Rossum, D.B., Patterson, R.L., Ma, H.T., and Gill, D.L. (2002). The cellular and molecular basis of store-operated calcium entry. Nat. Cell Biol. *4*, E263–E272.
15. Ma, H.T., Patterson, R.L., van Rossum, D.B., Birnbaumer, L., Mikoshiba, K., and Gill, D.L. (2000). Requirement of the inositol trisphosphate receptor for activation of store-operated Ca^{2+} channels. Science *287*, 1647–1651.
16. Ma, H.T., Venkatachalam, K., Li, H.S., Montell, C., Kurosaki, T., Patterson, R.L., and Gill, D.L. (2001). Assessment of the role of the inositol 1,4,5-trisphosphate receptor in the activation of transient receptor potential channels and store-operated Ca^{2+} entry channels. J. Biol. Chem. *276*, 18888–18896.
17. Bootman, M.D., Collins, T.J., Mackenzie, L., Roderick, H.L., Berridge, M.J., and Peppiatt, C.M. (2002). 2-aminoethoxydiphenyl borate (2-APB) is a reliable blocker of store-operated Ca^{2+} entry but an inconsistent inhibitor of $InsP_3$-induced Ca^{2+} release. FASEB J. *16*, 1145–1150.
18. Thastrup, O., Cullen, P.J., Drobak, B.K., Hanley, M.R., and Dawson, A.P. (1990). Thapsigargin, a tumor promoter, discharges intracellular Ca^{2+} stores by specific-inhibition of the endoplasmic-reticulum Ca^{2+}-ATPase. Proc. Natl. Acad. Sci. USA *87*, 2466–2470.
19. Bultynck, G., Sienaert, I., Parys, J.B., Callewaert, G., De Smedt, H., Boens, N., Dehaen, W., and Missiaen, L. (2003). Pharmacology of inositol trisphosphate receptors. Pflugers Arch. *445*, 629–642.
20. Broad, L.M., Braun, F.J., Lievremont, J.P., Bird, G.S.J., Kurosaki, T., and Putney, J.W. (2001). Role of the phospholipase C-inositol 1,4,5-trisphosphate pathway in calcium release-activated calcium current and capacitative calcium entry. J. Biol. Chem. *276*, 15945–15952.
21. Prakriya, M., and Lewis, R.S. (2001). Potentiation and inhibition of Ca^{2+} release-activated Ca^{2+} channels by 2-aminoethyldiphenyl borate (2-APB) occurs independently of IP_3 receptors. J. Physiol. (London) *536*, 3–19.
22. Kiselyov, K., Shin, D.M., Shcheynikov, N., Kurosaki, T., and Muallem, S. (2001). Regulation of Ca^{2+}-release-activated Ca^{2+} current (I_{crac}) by ryanodine receptors in inositol 1,4,5-trisphosphate-receptor- deficient DT40 cells. Biochem. J. *360*, 17–22.
23. Fierro, L., and Parekh, A.B. (1999). On the characterisation of the mechanism underlying passive activation of the Ca^{2+} release-activated Ca^{2+} current I_{CRAC} in rat basophilic leukaemia cells. J. Physiol. (London) *520*, 407–416.
24. Tsien, J.Z., Chen, D.F., Gerber, D., Tom, C., Mercer, E.H., Anderson, D.J., Mayford, M., Kandel, E.R., and Tonegawa, S. (1996). Subregion- and cell type-restricted gene knockout in mouse brain. Cell *87*, 1317–1326.
25. Marek, K.W., and Davis, G.W. (2002). Transgenically encoded protein photoinactivation (FlAsH-FALI): acute inactivation of synaptotagmin I. Neuron *36*, 805–813.
26. Poskanzer, K.E., Marek, K.W., Sweeney, S.T., and Davis, G.W. (2003). Synaptotagmin I is necessary for compensatory synaptic vesicle endocytosis in vivo. Nature *426*, 559–563.
27. Tour, O., Meijer, R.M., Zacharias, D.A., Adams, S.R., and Tsien, R.Y. (2003). Genetically targeted chromophore-assisted light inactivation. Nat. Biotechnol. *21*, 1505–1508.
28. Li, W.H., Schultz, C., Llopis, J., and Tsien, R.Y. (1997). Membrane-permeant esters of inositol polyphosphates, chemical syntheses and biological applications. Tetrahedron *53*, 12017–12040.

J|A|C|S
COMMUNICATIONS

Published on Web 12/24/2004

Design and Synthesis of Zinc-Selective Chelators for Extracellular Applications

Eri Kawabata,† Kazuya Kikuchi,†,‡ Yasuteru Urano,† Hirotatsu Kojima,† Akira Odani,§ and Tetsuo Nagano*,†

Graduate School of Pharmaceutical Sciences, The University of Tokyo, 7-3-1 Hongo, Bunkyo-ku,Tokyo 113-0033, Japan, Presto, JST Corporation, Kawaguchi, Saitama, Japan, and Department of Chemistry, Graduate School of Science, Nagoya University, Nagoya, Aichi, Japan

Received September 2, 2004; E-mail: tlong@mol.f.u-tokyo.ac.jp

Zinc (Zn^{2+}) is found in every cell in the human body and is mostly tightly bound to proteins as a key component of numerous enzymes and transcription factors.[1,2] Chelatable Zn^{2+} co-localizes with glutamate in the synaptic vesicles of certain glutamatergic vesicles in the mammalian brain, including the hippocampus, amygdala, and neocortex.[3] Free Zn^{2+} exists at a concentration of a few millimolar in the vesicles of presynaptic neurons and is released during synaptic activity or depolarization, modulating the function of certain ion channels and receptors.[4−7] Many reports describe the significance of Zn^{2+} in biological systems,[8−13] but its mechanisms of action are poorly understood.

Although various chemical tools for measuring Zn^{2+} in biological samples, such as fluorescence probes for Zn^{2+}, have been developed,[14−23] better Zn^{2+}-selective chelators are still needed. Research on Zn^{2+} signals in the brain has traditionally employed several chelators, though they have various shortcomings for biological applications. Use of *N,N,N′,N′*-tetrakis(2-pyridylmethyl)-ethylenediamine (TPEN), a classical membrane-permeable Zn^{2+} chelator, does not allow selective manipulation of extracellular or intracellular Zn^{2+}. On the other hand, calcium ethylenediaminetetraacetic acid (CaEDTA), an extracellular (membrane-impermeable) Zn^{2+} chelator, has the disadvantage of slow kinetics of Zn^{2+} binding. Concentrations of CaEDTA that are sufficient to chelate synaptic Zn^{2+} at equilibrium do not effectively chelate Zn^{2+} within the period of tens to hundreds of microseconds that it takes Zn^{2+} to cross the synapse and interact with various postsynaptic sites.[24] In contrast, a higher concentration of CaEDTA markedly reduces the Zn^{2+} and Ca^{2+} signals.[25] This phenomenon makes it difficult to interpret the action mechanism of Zn^{2+} under physiological conditions, where change of Ca^{2+} concentration can also induce various responses. Especially in electrophysiological studies of ion channels and neuronal activities, reduction of extracellular Ca^{2+} can result in neurological side effects. The development of new, more rapid Zn^{2+} chelators which have low affinity for Ca^{2+} is required for the clarification of the mechanism of synaptic release of Zn^{2+}. We report here the design, synthesis, and properties of new Zn^{2+} chelators, and we describe biological application in hippocampal slices.

We designed (4-{[2-(bis-pyridin-2-ylmethylamino)ethylamino]-methyl}phenyl)methanesulfonic acid, sodium salt (DPESA), and [4-({[2-(bis-pyridin-2-ylmethylamino)ethyl]pyridin-2-ylmethylamino}-methyl)phenyl]methanesulfonic acid, sodium salt (TPESA) utilizing TPEN structure for high Zn^{2+} selectivity and a sulfonic acid moiety for hydrophilicity (Figure 1). The acid dissociation constants and metal chelate stability constants were determined by potentiometric methods (Table 1 and Table S1, Supporting Information). The log K values of DPESA and TPESA for Zn^{2+} are 11.8 and 12.3, respectively, showing that these two compounds have high affinity for Zn^{2+}. The log K values for Ca^{2+} are 4.20 and 2.47, and those for Mg^{2+} are 3.97 and 2.66, respectively, indicating low affinity for these metal ions.

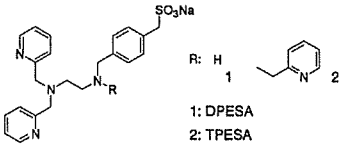

Figure 1. Structures of new zinc-selective chelators.

Table 1. Stability Constants of Chelators

	log K			
M^{n+}	DPESA[a]	TPESA[a]	TPEN[b]	EDTA[b]
Ca^{2+}	4.20 ± 0.11	2.47 ± 0.10	4.40	10.7
Mg^{2+}	3.97 ± 0.10	2.66 ± 0.10	1.70	8.64
Zn^{2+}	11.8 ± 0.01	12.3 ± 0.03	15.4	16.3

[a] Stability constants of DPESA and TPESA were determined at 25 °C, I = 0.1. The determined value ± SD is given. [b] From the SCDatabase (IUPAC and Academic Software): 25 °C, I = 0.1.

To compare the relative association rate constants of the new chelators for Zn^{2+} with those of traditional chelators, competition analysis was performed between Zn^{2+}-fluorescence probe complex and Zn^{2+}-selective chelators (Figure S3, Supporting Information). ZnAF-2[14a] was used as a fluorescence probe for Zn^{2+}; its log K_{obs} value (K_{obs} is the apparent association constant at pH 7.4, I = 0.10 M $NaNO_3$) has been reported as 8.57. The fluorescence intensity of ZnAF-2 (1.0 μM) linearly increased up to a 1:1 [ZnAF-2]/[Zn^{2+}] ratio, and the maximum fluorescence was obtained with 1.0 μM Zn^{2+} addition. Then 10 μM chelator was added and the time course of fluorescence decrease was compared among DPESA, TPESA, TPEN, and CaEDTA. The addition of 10 μM TPESA rapidly decreased the fluorescence with a half-life of 18.6 s, which is comparable to that of TPEN (12.2 s). This result suggested that TPESA can reduce the concentration of synaptically released Zn^{2+} rapidly, without changing the extracellular Ca^{2+} concentration. On the other hand, DPESA reduced the fluorescence with a half-life of 67.0 s, which is similar to the value of 65.4 s obtained for CaEDTA. Considering that DPESA may have the same affinity for Zn^{2+} as ZnAF-2, whereas the other chelators have higher affinities (Table 1), the above result suggests rapid Zn^{2+} chelation.

To examine the membrane permeability of the new chelators, we applied them to hippocampal slices (Figure S4, Supporting Information). Acute rat hippocampal slices were incubated with 10 μM ZnAF-2 DA[14a] for 1.5 h at room temperature for dye loading.

† The University of Tokyo.
‡ Presto, JST Corporation.
§ Nagoya University.

10.1021/ja044697q CCC: $30.25

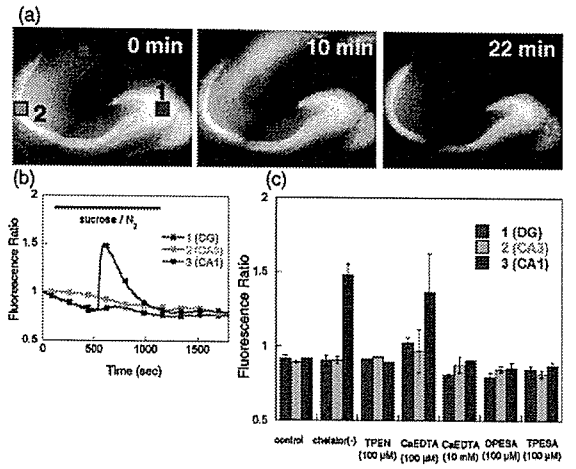

Figure 2. Application of the chelators under ischemic conditions. Dye-loaded slices were exposed to anoxic-aglycemiic ACSF for 17 min (from 2 to 19 min). (a) Fluorescence images at 0, 10, and 22 min after the measurement. The fluorescence ratio in the plot (b) is the ratio of the fluorescence intensity to the initial intensity of the corresponding area in the image at 0 min. (c) Histogram showing the effects of the chelators on the fluorescence change of ZnAF-2 DA-loaded slices under anoxia-aglycemia. Fluorescence ratio in the histogram is the ratio of the fluorescence intensity at 10 min after the start of the measurement to the initial intensity of the corresponding area in the image at 0 min. Each column, except for TPEN, shows the mean ± SE.

ZnAF-2 DA is expected to permeate well through the cell membrane and then to be transformed to ZnAF-2 by esterase in the cytosol, where the dye would be retained for a long time. It interacts with intracellular Zn^{2+} to generate strong fluorescence. The fluorescence was intense in the hilus and the stratum lucidum of the CA3 region, where Zn^{2+} is concentrated in the vesicles.[6] The fluorescence was decreased by extracellular addition of the membrane-permeable chelator TPEN (100 μM) for 30 min, whereas it was scarcely altered by addition of CaEDTA, DPESA, or TPESA. These results support the view that DPESA and TPESA are membrane-impermeable chelators.

It has been suggested that the concentration of intracellular Zn^{2+} at the hippocampal CA1 region transiently increases in response to an ischemic insult, which is content with a relationship between Zn^{2+} and apoptosis.[14b] This increase might be derived from influx of extracellular Zn^{2+} released from the presynaptic terminals, or from the release of Zn^{2+} from intracellular vesicles. To investigate the second possibility, we used DPESA and TPESA (Figure 2).

Acute rat hippocampal slices which had been loaded with ZnAF-2 DA were exposed to anoxic-aglycemic ACSF for 17 min. The fluorescence in the CA1 region increased transiently, but this was not observed when TPEN (100 μM) was added extracellularly (30-min preperfusion with 100 μM TPEN followed by anoxic-aglycemic insult in the presence of 100 μM TPEN). Similarly, the presence of 100 μM DPESA or TPESA inhibited the transient increase in fluorescence, indicating that DPESA and TPESA chelated synaptically released Zn^{2+} quite rapidly and thereby suppressed influx of Zn^{2+} into the cells. These results suggest that Zn^{2+} is released from the presynaptic vesicles in response to an ischemic insult and is taken up intracellularly into the postsynaptic neurons. Notably, 100 μM DPESA or TPESA was sufficient for Zn^{2+} chelation, whereas 100 μM CaEDTA was not. Thus, our newly designed chelators yielded the biologically significant finding that presynaptic Zn^{2+} can be released in the CA1 region. This confirms the utility of these new chelators as extracellular Zn^{2+} chelators for biological applications.

In conclusion, we have developed new membrane-impermeable Zn^{2+}-selective chelators, DPESA and TPESA, with the advantageous characteristics of high Zn^{2+} selectivity and rapid chelation, that can be applied to cell-biological studies to shed additional light on the function of synaptically released Zn^{2+}.

Acknowledgment. This work was supported in part by the Ministry of Education, Culture, Sports, Science and Technology of Japan (Grant Nos. 16370071 to T.N., 15681012 and 16048206 to K.K.). K.K. was also supported by the Sankyo Foundation, the Kanagawa Academy of Science, and the Suzuken Memorial Foundation.

Supporting Information Available: Synthesis, experimental details, and characterization of DPESA and TPESA. This material is available free of charge via the Internet at http://pubs.acs.org.

References

(1) Vallee, B. L.; Falchuk, K. H. *Physiol. Rev.* **1993**, *73*, 79−118.
(2) O'Halloran, T. V. *Science* **1993**, *261*, 715−725.
(3) Frederickson, C. J. *Int. Rev. Neurobiol.* **1989**, *31*, 145−238.
(4) Weiss, J. H.; Sensi, S. L.; Koh, J.-Y. *Trends Pharmacol. Sci.* **2000**, *21*, 395−401.
(5) Molnar, P.; Nadler, J. V. *Brain Res.* **2001**, *910*, 205−207.
(6) Ueno, S.; Tsukamoto, M.; Hirano, T.; Kikuchi, K.; Yamada, M.; Nishikawa, N.; Nagano, T.; Matsuki, N.; Ikegaya, Y. *J. Cell Biol.* **2002**, *158*, 215−220.
(7) Hosie, A. M.; Dunne, E. L.; Harvey, R. J.; Smart, T. G. *Nat. Neurosci.* **2003**, *6*, 362−369.
(8) Bush, A. I.; Pettingel, W. H.; Multhaup, G.; Paradis, M. D.; Vonsattel, J. P.; Gusella, J. F.; Beyreuther, K.; Masters, C. L.; Tanzi, R. E. *Science* **1994**, *265*, 1464−1467.
(9) Koh, J.-Y.; Suh, S. W.; Gwag. B. J.; He, Y. Y.; Hsu, C. Y.; Choi, D. W. *Science* **1996**, *272*, 1013−1016.
(10) Truong-Tran, A. Q.; Ho, L. H.; Chai, F.; Zalewski, P. D. *J. Nutr.* **2000**, *130*, 1459S−1466S.
(11) (a) Suh, S. W.; Chen, J. W.; Motamedi, M.; Bell, B.; Listiak, K.; Pons, N. F.; Danscher, G.; Frederickson, C. J. *Brain Res.* **2000**, *852*, 268−273. (b) Li, Y.; Hough, C. J.; Suh, S. W.; Sarvey, J. M.; Frederickson, C. J. *J. Neurophysiol.* **2001**, *86*, 2597−2604.
(12) Truong-Tran, A. Q.; Carter, J.; Ruffin, R. E.; Zalewski, P. D. *BioMetals* **2001**, *14*, 315−330.
(13) Kay, A. R. *J. Neurosci.* **2003**, *23*, 6847−6855.
(14) (a) Hirano, T.; Kikuchi, K.; Urano, Y.; Higuchi, T.; Nagano, T. *J. Am. Chem. Soc.* **2000**, *122*, 12399−12400. (b) Hirano, T.; Kikuchi, K.; Urano, Y.; Nagano, T. *J. Am. Chem. Soc.* **2002**, *124*, 6555−6562.
(15) Tompson, R. B.; Whetsell, W. O., Jr.; Maliwal, B. P.; Fierke, C. A.; Frederickson, C. J. *J. Neurosci. Methods* **2000**, *96*, 35−45.
(16) (a) Walkup, G. K.; Imperiali, B. *J. Am. Chem. Soc.* **1996**, *118*, 3053−3054. (b) Pearce, D. A.; Jotterand, N.; Carrico, I. S.; Imperiali, B. *J. Am. Chem. Soc.* **2001**, *123*, 5160−5161. (c) Shults, M. D.; Pearce, D. A.; Imperiali, B. *J. Am. Chem. Soc.* **2003**, *125*, 10591−10597.
(17) (a) Fahrni, C. J.; O'Halloran, T. V. *J. Am. Chem. Soc.* **1999**, *121*, 11448−11458. (b) Taki, M.; Wolford, J. L.; O'Halloran, T. V. *Am. Chem. Soc.* **2004**, *126*, 712−713.
(18) (a) Fahrni, C. J.; Henary, M. M.; VanDerveer D. G. *J. Phys. Chem. A* **2002**, *106*, 7655−7663. (b) Henary, M. M.; Wu, Y.; Fahrni, C. J. *Chem. Eur. J.* **2004**, *10*, 3015−3025.
(19) (a) Walkup, G. K.; Burdette, S. C.; Lippard, S. J.; Tsien, R. Y. *J. Am. Chem. Soc.* **2000**, *122*, 5644−5645. (b) Burdette, S. C.; Walkup, G. K.; Spingler, B.; Tsien, R. Y.; Lippard, S. J. *J. Am. Chem. Soc.* **2001**, *123*, 7831−7841. (c) Burdette, S. C.; Frederickson, C. J.; Lippard, S. J. *J. Am. Chem. Soc.* **2003**, *125*, 1778−1787.
(20) (a) Gee, K. R.; Zhou, Z. L.; Qian, W. J.; Kennedy, R. *J. Am. Chem. Soc.* **2002**, *124*, 776−778. (b) Sensi, S. L.; Ton-That, D.; Weiss, J. H.; Rothe, A.; Gee, K. R. *Cell Calcium* **2003**, *34*, 281−284.
(21) Godwin, H. A.; Berg, J. M. *J. Am. Chem. Soc.* **1996**, *118*, 6514−6515.
(22) Budde, T.; Minta, A.; White, J. A.; Kay, A. R. *Neuroscience* **1997**, *79*, 347−358.
(23) Haugland, R. P. *Handbook of Fluorescent Probes and Research Products*, 8th ed.; Molecular Probes, Inc.: Eugene, OR, 2001; Section 20.7.
(24) Vogt, K.; Mellor, J.; Tong, V.; Nicoll, R. *Neuron* **2000**, *26*, 187−196.
(25) Li, Y.; Hough, C. J.; Frederickson, C. J.; Sarvey, J. M. *J. Neurosci.* **2001**, *21*, 8015−8025.

JA044697Q

Gene Therapy (2005) 12, 203–210

www.nature.com/gt

RESEARCH ARTICLE

Efficient and stable Sendai virus-mediated gene transfer into primate embryonic stem cells with pluripotency preserved

K Sasaki[1,2], M Inoue[3], H Shibata[1], Y Ueda[3], S-i Muramatsu[4], T Okada[1], M Hasegawa[3], K Ozawa[1] and Y Hanazono[1]

[1]*Center for Molecular Medicine, Jichi Medical School, Minamikawachi, Tochigi, Japan;* [2]*Department of Plastic and Reconstructive Surgery, Faculty of Medicine, University of Tokyo, Bunkyo-ku, Tokyo, Japan;* [3]*DNAVEC Corporation, Tsukuba, Ibaraki, Japan; and* [4]*Department of Neurology, Jichi Medical School, Minamikawachi, Tochigi, Japan*

Efficient gene transfer and regulated transgene expression in primate embryonic stem (ES) cells are highly desirable for future applications of the cells. In the present study, we have examined using the nonintegrating Sendai virus (SeV) vector to introduce the green fluorescent protein (GFP) gene into non-human primate cynomolgus ES cells. The GFP gene was vigorously and stably expressed in the cynomolgus ES cells for a year. The cells were able to form fluorescent teratomas when transplanted into immunodeficient mice. They were also able to differentiate into fluorescent embryoid bodies, neurons, and mature blood cells. In addition, the GFP expression levels were reduced dose-dependently by the addition of an anti-RNA virus drug, ribavirin, to the culture. Thus, SeV vector will be a useful tool for efficient gene transfer into primate ES cells and the method of using antiviral drugs should allow further investigation for regulated SeV-mediated gene expression.
Gene Therapy (2005) **12,** 203–210. doi:10.1038/sj.gt.3302409
Published online 14 October 2004

Keywords: *primate embryonic stem cell; Sendai virus vector; gene transfer; green fluorescent protein; pluripotency; ribavirin*

Introduction

Since human embryonic stem (ES) cell lines have the ability to both proliferate indefinitely and differentiate into multiple tissue cells,[1,2] they are expected to have clinical applications as well as to serve as models for basic research and drug development. Although efficient and stable gene transfer into primate ES cells would be useful for such purposes, it has been difficult and only lentiviral vectors have been successful in achieving it.[3–5] We have previously developed Sendai virus (SeV) vectors that replicate in the form of negative-sense single-stranded RNA in the cytoplasm of infected cells and do not go through a DNA phase.[6] SeV vectors can efficiently introduce foreign genes without toxicity into airway epithelial cells,[7] vascular tissue,[8] skeletal muscle,[9] synovial cells,[10] retinal tissue,[11] and hematopoietic progenitor cells.[12] Here we report that the SeV-mediated gene transfer into primate ES cells is very efficient and stable even after the terminal differentiation of the cells. In addition, we show that SeV-mediated transgene expression levels can be reduced by the addition of a ribonucleoside analog, ribavirin, to the culture. Ribavirin is a mutagen and inhibitor of viral RNA polymerase.[13,14] It shows antiviral activity against a variety of RNA viruses and is used to treat infections of hepatitis C virus in combination with interferon-α[15,16] and of lassa fever virus.[17] The method of using antiviral drugs might offer a novel approach for regulated SeV-mediated gene expression in primate ES cells.

Correspondence: Dr Y Hanazono, Center for Molecular Medicine, Jichi Medical School, 3311-1 Yakushiji, Minamikawachi, Tochigi 329-0498, Japan
Received 20 April 2004; accepted 27 August 2004; published online 14 October 2004

Results

SeV-mediated gene transfer into ES cells

In this study, we have used an SeV vector, which is capable of self-replication but incapable of transmitting to other cells.[6] The vector does not encode the fusion (F) protein (Figure 1a), which is essential for viral entry into cells. It can be propagated only in a packaging cell line expressing the F protein. The green fluorescent protein (GFP) gene was introduced after the leader sequence of the vector genome. Cynomolgus ES cells[18] were exposed to the SeV vector for 24 h. Flow cytometric analysis at 2 days after infection showed that 15, 38, and 61% of cells fluoresced at 2, 10, and 50 transducing units (TU) per cell, respectively (Figure 1b). The gene transfer efficiency of about 60% is comparable to or even better than that for lentiviral vectors.[3] We confirmed that the undifferentiated cell fractions remained unchanged after the infection with SeV vector, as assessed by the expression of undifferentiated markers, alkaline phosphatase and SSEA-4 (data not shown). The GFP expression after infection was stable at least for a month. On the other hand, the GFP gene transfer to cynomolgus ES cells with adenovirus- and adeno-associated virus (AAV)-based vectors resulted in much lower expression levels (<20% by flow cytometry) and the levels declined to zero within a week after infection (Figure 1c).

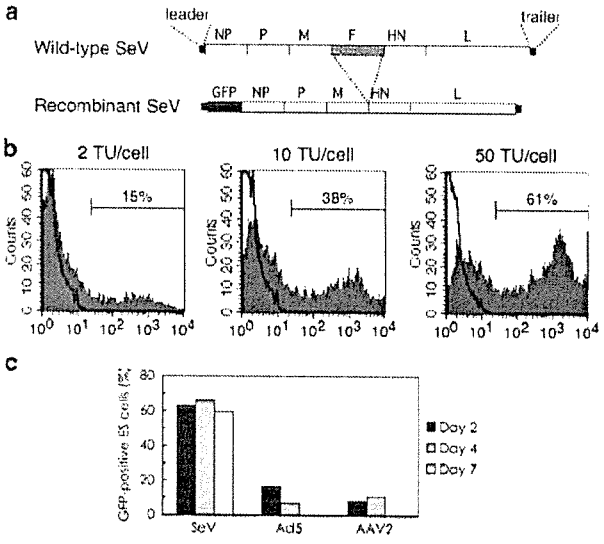

Figure 1 High-level transgene expression in cynomolgus ES cells after infection with SeV vector. (a) Schematic diagrams of the wild-type SeV genome and recombinant F-defective SeV carrying the GFP gene (SeV vector in this study). The SeV genome is 15 384 nucleotides long and its genes (NP, P, M, F, HN, and L) are in order from 3′ to 5′ in the negative-strand RNA. In the SeV vector, the entire fusion (F) gene was removed and the GFP gene was introduced at a unique NotI site between the leader sequence and NP gene. (b) The GFP expression by the SeV vector in cynomolgus ES cells. Cynomolgus ES cells were infected with the SeV vector at 2, 10, and 50 TU/cell. The flow cytometric profiles at day-2 postinfection are shown in gray. The white areas indicate uninfected ES cells. The fractions of GFP-positive cells are indicated. (c) The GFP expression levels in cynomolgus ES cells infected with the SeV (50 TU/cell), adenovirus serotype 5 (Ad5, 3.4×10^2 g.c./cell), and AAV serotype 2 (AAV2, 2.4×10^4 g.c./cell) vectors. The fractions of GFP-positive cells were examined by flow cytometry at 2, 4, and 7 days postinfection.

We plucked fluorescent ES cell colonies under a fluorescent microscope once at 1 month after infection and propagated them. After this selection procedure, approximately 90% of the ES cells expressed GFP (Figure 2a and b) and the high-level expression was stable for a year as assessed by flow cytometry (Figure 2c, upper). The mean fluorescence intensity per cell was also stable (Figure 2c, lower), indicating that the replicating vector genome was almost equally delivered to each cell of all progeny. The self-replication of the SeV vector in infected cells was confirmed by RNA-PCR that amplified the viral RNA genomic sequence (Figure 3a). The GFP cDNA sequence, however, could not be detected by DNA-PCR in the infected cells (Figure 3b), indicating that no DNA phase was involved in the GFP expression.

Pluripotency of infected ES cells

The SeV-infected, fluorescent cynomolgus ES cells were able to form fluorescent tumors when transplanted into immunodeficient mice (Figure 4a–c). The fluorescence was observed uniformly by fluorescent microcopy (Figure 4d and e). The tumors consisted of all three embryonic germ layer cells (Figure 4f–i). Thus, the SeV-infected ES cells were capable of forming teratomas and the SeV infection did not spoil the pluripotency of ES cells. The infected, fluorescent cynomolgus ES cells were also able to generate fluorescent embryoid bodies (Figure 5a and b), MAP-2-positive neurons (Figure 5c), clonogenic hematopoietic colonies (Figure 5d and e), and mature functional (NBT test-positive) neutrophils (Figure 5f and g), all of which fluoresced. In addition, the GFP expression levels were not decreased during the teratoma formation or differentiation, indicating that no 'silencing' of the transgene occurred.

Drug-inducible reduction of transgene expression

Next, we examined whether ribavirin inhibits the replication and transcription of the SeV vector resulting in a reduction of transgene expression. We first used a rhesus monkey kidney cell line (LLC-MK2) to test the effect of ribavirin on the replication and transcription of the SeV vector. LLC-MK2 is a standard control cell line for SeV infection. Ribavirin was added at various concentrations 2 days after the infection. The formation of viral particles quantified by the hemagglutination assay decreased drastically upon the addition of ribavirin (Figure 6a). The decrease was dependent on the dose of ribavirin. The GFP expression was also depressed dose-dependently (Figure 6b). Thus, ribavirin dose-dependently inhibits the replication and transcription of the SeV vector in LLC-MK2 cells. The toxicity associated with ribavirin was not observed in LLC-MK2 cells.

We then examined the effect of ribavirin on SeV-infected, fluorescent cynomolgus ES cells. The addition of ribavirin also resulted in a dose-dependent reduction of GFP expression in the cells (Figure 6c). Although the GFP expression was almost completely inhibited after a 3-day exposure with 4 mM of ribavirin, the cells could not be propagated thereafter. Ribavirin at high concentrations (>1 mM) hampered the proliferation of cynomolgus ES cells. With lower concentrations (0.5–0.75 mM) of ribavirin, the GFP expression level decreased by half. After the discontinuation of ribavirin treatment, the cells could be propagated and nearly regained the original level of GFP expression. The undifferentiated cell fractions were unchanged after the discontinuation as assessed by alkaline phosphatase and SSEA-4 staining (Figure 6d).

Discussion

There are several advantages in using SeV vectors over other vectors. (i) SeV vectors can infect nondividing, quiescent cells as well as dividing cells unlike oncoretroviral vectors.[7–11] Thus, they can be used to infect cells that are terminally differentiated as well as at various stages of differentiation, whether they are dividing or not. (ii) SeV vector-mediated gene transfer does not require a DNA phase. Thus, there is no concern about the unwanted integration of foreign sequences into the host genome unlike with oncoretroviral or lentiviral vectors. (iii) Transgene expression is stable even in dividing cells since the SeV vector replicates by itself in the cytoplasm of host cells. On the other hand, gene transfer using nonreplicating adenoviral and AAV vectors resulted in decreased levels of transgene expression in dividing cells over time, since the non-replicating transgene was

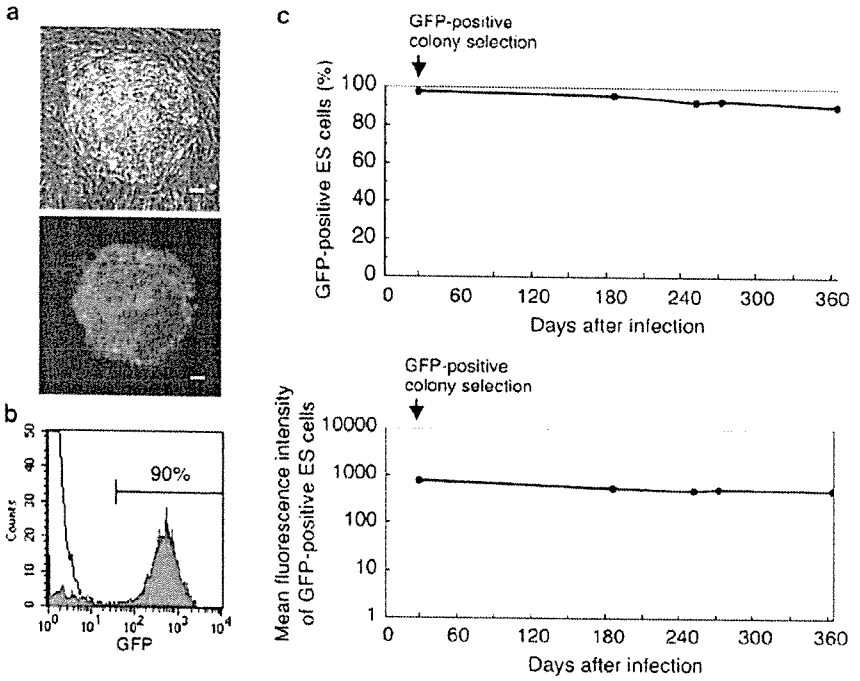

Figure 2 Stable SeV-mediated transgene expression in cynomolgus ES cells. Fluorescent ES cell colonies were plucked under a fluorescent microscope once at 1 month after infection and the cells were further propagated. (a) Phase-contrast (upper) and fluorescence (lower) images of a cynomolgus ES cell colony at day 370 after infection. Bar = 100 μm. (b) Flow cytometric analysis of SeV-infected cynomolgus ES cells at day 370 after infection (shown in green). The percentage of GFP-positive cells is indicated. Uninfected, parental cynomolgus ES cells are indicated by another line (white area). (c) The percentage of GFP-positive cells (upper) and mean fluorescence intensity per GFP-positive cell (lower) after infection with the SeV vector at 10 TU/cell are shown as a function of time (days).

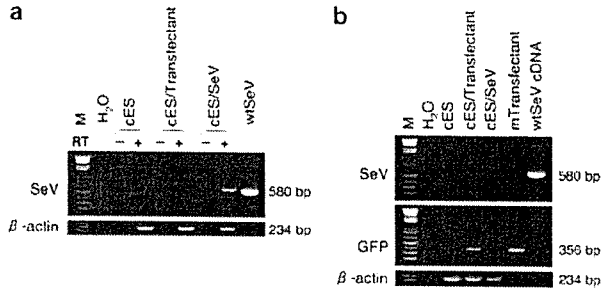

Figure 3 DNA-independent replication and transcription of SeV vector. Total cellular RNA and DNA were extracted from cynomolgus ES cells at day 284 after infection with the SeV vector. RNA-PCR (a) and DNA-PCR (b) for the SeV RNA genome or GFP sequence were conducted. The cynomolgus β-actin sequence was used as an internal control. In the RNA-PCR (a), negative results obtained without reverse transcriptase (designated RT−) confirmed that the amplified products were not derived from cellular DNA. M, 100-kb DNA ladder; cES, naive cynomolgus ES cells; cES/Transfectant, cynomolgus ES cells stably expressing the GFP gene after transfection,[33] cES/SeV, cynomolgus ES cells infected with the SeV vector; wtSeV, wild-type SeV genome; mTransfectant, a GFP-positive mouse cell line after transfection.

diluted out. (iv) The SeV vector is much less unlikely to generate wild-type virus *in vitro* or *in vivo* than oncoretroviral and lentiviral vectors, since homologous recombination between RNA genomes is very rare indeed in negative-strand RNA viruses.[19] (v) The SeV genome is not subject to cellular epigenetic modifications such as methylation, and thus it is unlikely that methylation-based silencing of transgene expression occurs.

No cytotoxic or differentiating effect on ES cells associated with the SeV infection was observed in our study. However, the wild-type SeV contains immunogenic surface proteins, hemagglutinin-neuraminidase (HN) and F proteins, which potentially induce antibody responses.[20,21] For future clinical applications, it would be desired that as many viral genes as possible are deleted from the vector backbone to permit reapplication, improve the safety, and lessen the possible toxicity of SeV vectors. To this end, we have developed a series of attenuated SeV vectors that are F gene-deleted,[6] F gene-deleted with preferable mutations,[22] M gene-deleted,[23] or have deletions of both F and M genes.[24] The modified vectors would be safer for *in vivo* use.

Ribavirin at high concentrations seems toxic to ES cells; presumably, it directly hampers viability and proliferation potential of ES cells. However, we cannot tell whether the observed toxicity is simply due to its toxicity to ES cells, as feeder cells are more highly sensitive to ribavirin than ES cells. In fact, while feeder cells died at 1 mM of ribavirin, cocultured ES cells were alive at this concentration for some time. Cynomolgus ES cells lose pluripotency and proliferation potential without feeder cells. Thus, the observed toxicity to ES cells may also be a secondary event following the injury of feeder cells. Whether the cytotoxicity is primary or secondary, it will be necessary to find modified compounds of less cytotoxicity.

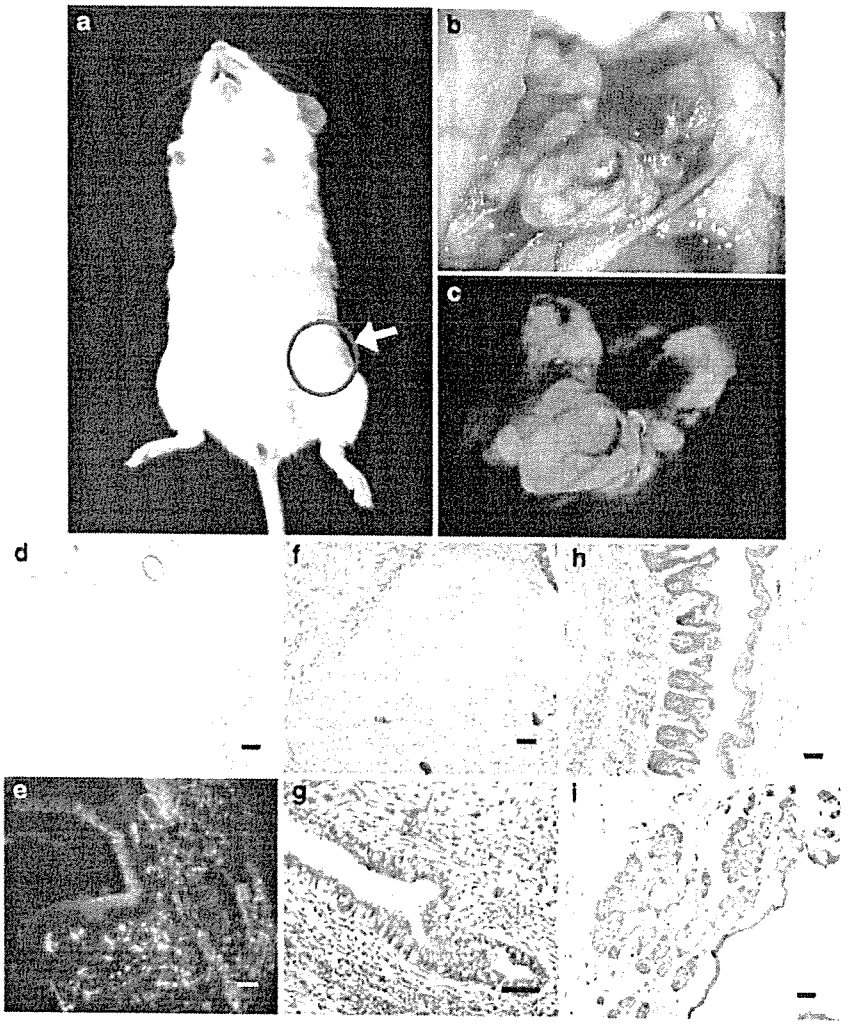

Figure 4 Pluripotency of SeV-infected cynomlgus ES cells. Tumors formed in NOD-SCID mice after inoculation of the SeV-infected cynomolgus ES cells (a). The tumor was fluorescing ((b), bright field; (c), dark field). Fluorescence was observed uniformly in the tumor under a fluorescent microscope ((d), bright field; (e), dark field). The tumor contained all three embryonic germ layer cells; cartilage (f), ciliated columnar epithelium (g), skin (h), and sebaceous gland (i) (stained with hematoxylin and eosin). Bar = 100 μm.

Materials and methods

Cell culture

Cynomolgus ES cells (CMK6) were maintained on a feeder layer of mitomycin C (Kyowa, Tokyo, Japan)-treated mouse (BALB/c) embryonic fibroblasts as described previously.[18] The culture medium consisted of Dulbecco's modified Eagle's medium (DMEM)/F12 (Invitrogen, Carlsbad, CA, USA) supplemented with 15% ES cell-qualified fetal calf serum (FCS; Invitrogen), 0.1 mM 2-mercaptoethanol (Sigma, St Louis, MO, USA), 2 mM glutamine (Invitrogen), 0.1 mM nonessential amino acids (Invitrogen), and antibiotics (100 U/ml penicillin and 100 μg/ml streptomycin, Irvine Scientific, Santa Ana, CA, USA). The ES cell colonies were routinely passaged every 3–4 days after dissociation with a combined approach of 0.25% trypsin (Invitrogen) digestion and mechanical cutting. Alkaline phosphatase staining was conducted with an Alkaline Phosphatase Chromogen Kit (Biomeda, Foster City, CA, USA). Embryoid bodies were produced by culturing ES cell aggregates in Petri dishes. LLC-MK2 cells (1×10^6) were grown in six-well plates and cultured in Eagle's minimal essential medium (Invitrogen) supplemented with 10% FCS.

Vectors

The F-defective SeV vector carrying the GFP gene was constructed as previously described.[6] The vector titer was 1.8×10^9 TU/ml determined by counting fluorescent cells after the infection of LLC-MK2 cells. Gene transfer was conducted by adding various concentrations of the SeV vector solution to culture media. After 24 h of incubation, the cells were washed twice with phosphate-buffered saline (PBS) and fresh medium was added. In some experiments, ribavirin (1-β-D-ribofuranosyl-1,2,4-triazole-3-carboxamide; Sigma) was added at various concentrations to the culture media after infection. The

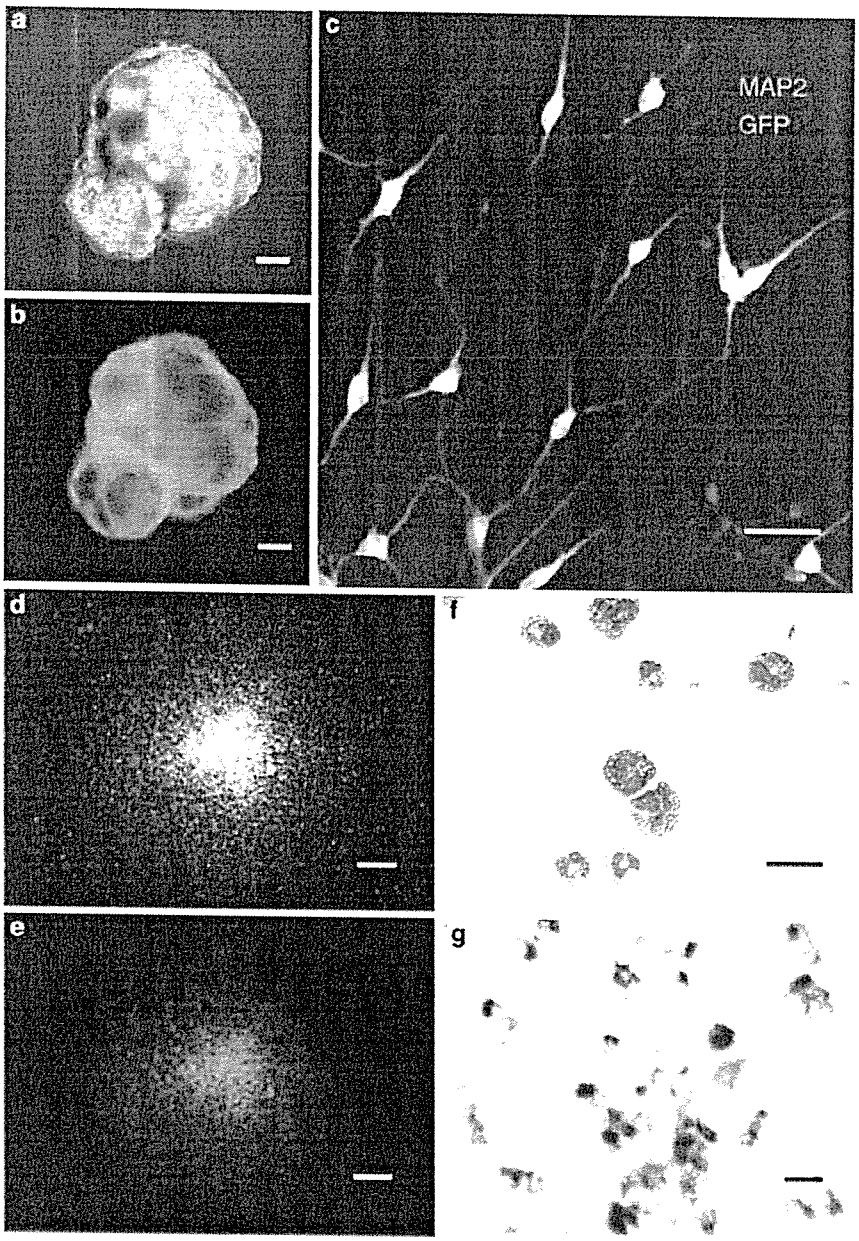

Figure 5 Stable transgene expression during differentiation. A day-20 cystic embryoid body was observed under a fluorescent phase-contrast microscope, confirming that the embryoid body was fluorescing ((a), bright field; (b), dark field). After infection with the SeV vector, fluorescent cynomolgus ES cells differentiated into neural cells. Double immunostaining with anti-GFP (green) and ant-MAP-2 (red) confirmed that differentiated neural cells expressed GFP (c). Yellow cells indicate GFP-expressing neurons. SeV-infected, fluorescent cynomolgus ES cells also differentiated into fluorescent hematopoietic cells. A clonogenic hematopoietic colony was fluorescing ((d) bright field; (e), dark field). A cytospin specimen of hematopoietic colony cells (Wright–Giemsa staining) showed that the cells were mature granulocytes (f). The infected ES cell-derived, fluorescent neutrophils were positive for NBT (stained in black (g)). Bar = 100 μm (a, b, g); 50 μm (c, f); 500 μm (d, e).

viral particles in infected cells were quantified by a hemagglutination assay as described previously.[25]

An adenovirus serotype 5-based vector carrying the GFP gene was constructed as reported.[26] It contained the cytomegalovirus (CMV) promoter, simian virus (SV)-40 intron, and SV-40 polyadenylation signal. An AAV serotype 2-based vector expressing the GFP gene under the control of the chicken β-actin promoter with the CMV immediate-early enhancer (a gift from Dr J Miyazaki) was prepared as described previously.[27] Gene transfer experiments were performed using 3.4×10^2 genome copies (g.c.)/cell of the adenoviral vector or 2.4×10^4 g.c./cell of the AAV vector. The period of exposure was 48 h.

Flow cytometry

GFP and SSEA-4 expression was analyzed on a FACScan (Becton Dickinson, Franklin Lakes, NJ, USA) using the

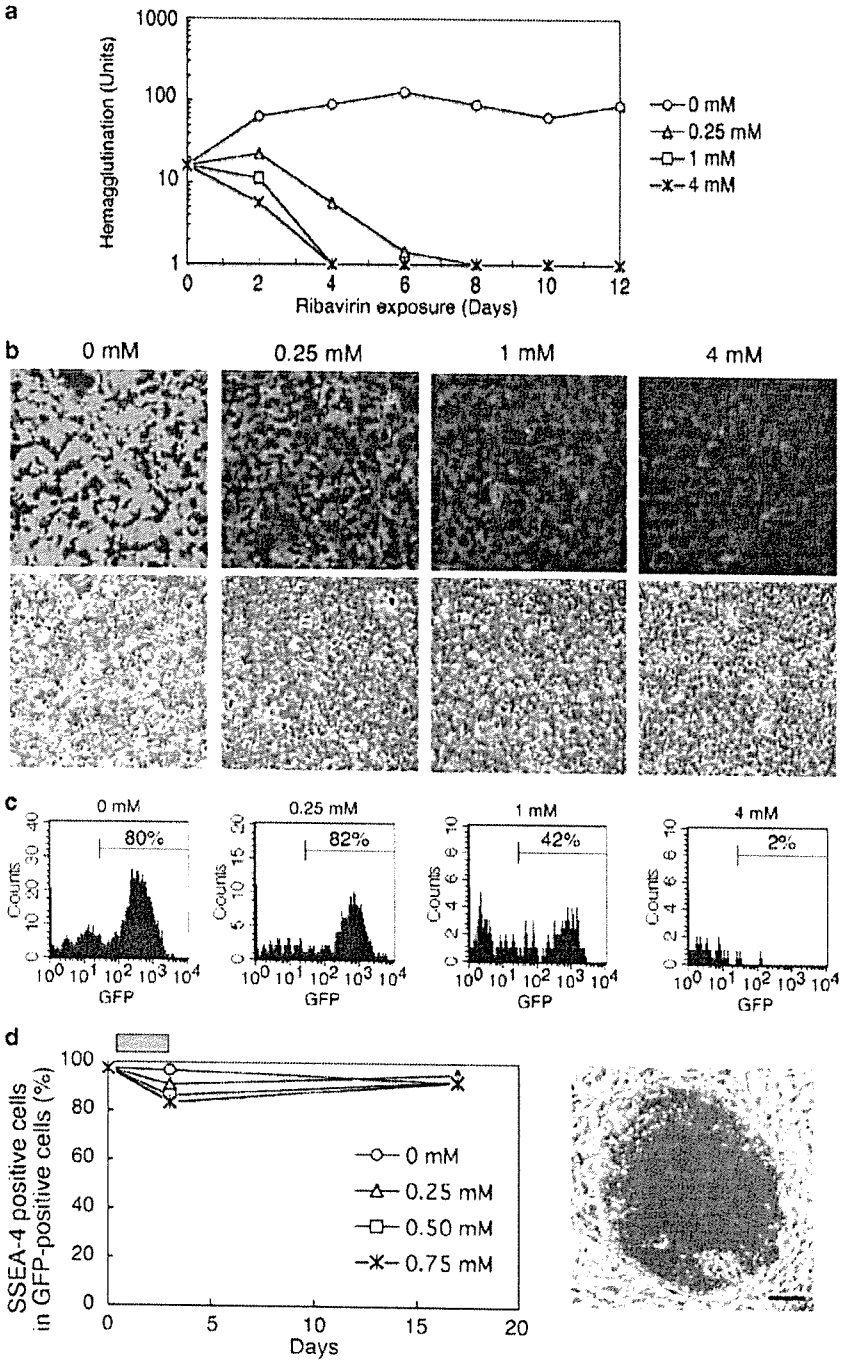

Figure 6 Ribavirin-regulated transgene expression. (a) A rhesus kidney cell line (LLC-MK2) was infected with the SeV vector at 3 TU/cell. Ribavirin was started at various concentrations on day 2 after the infection. The formation of viral particles in the infected LLC-MK2 cells was examined by the hemagglutination assay. (b) The ribavirin-treated LLC-MK2 cells were observed under a fluorescent microscope after an 8-day exposure of ribavirin (upper, dark field; lower, bright field). (c) Ribavirin was added at various concentrations to the SeV-infected, fluorescent cynomolgus ES cells. The GFP expression was assessed by flow cytometry after a 3-day exposure of ribavirin. (d) The fractions of SSEA-4-positive ES cells were assessed by flow cytometry with anti-SSEA-4 before and after a 3-day exposure of ribavirin and are shown as a function of time (days) in the left panel. A gray bar indicates ribavirin treatment. ES cells were stained for alkaline phosphatase (in red) at day 21 after a 3-day exposure of 0.75 mM ribavirin and are shown in the right panel. Bar = 100 μm.

CellQuest software (Becton Dickinson). For SSEA-4 staining, cells were incubated with a primary antibody, anti-SSEA-4 (MC-813-70; Chemicon, Temecula, CA, USA), and then a secondary antibody, PE-conjugated F(ab')2 fragment of rabbit anti-mouse immunoglobulins (DakoCytomation, Glostrup, Denmark). Cocultured BALB/c feeder cells could be distinguished from cynomolgus ES cells by using PE-conjugated anti-mouse

H-2d (SF1-1.1; PharMingen, San Diego, CA, USA), which does not react to cynomolgus cells but does react to BALB/c cells.

Teratoma formation

Cynomolgus ES cells (approximately 10^6 cells per site) were injected subcutaneously into the hind leg of 6- to 8-week-old nonobese diabetic/severe combined immunodeficient mice (Jackson Laboratory, Bar Harbor, ME, USA). The resulting tumors (usually 9–12 weeks after the injection) were dissected and fixed in 4% paraformaldehyde. For histological analysis, samples from the tumors were embedded in paraffin and stained with hematoxylin and eosin. To observe GFP fluorescence, samples were embedded in OTC compound (Sakura, Zoeterwoude, Netherlands), frozen, sectioned, and examined under a fluorescence microscope.

Hematopoietic differentiation

The mouse bone marrow stromal cell line OP9 was maintained in α-modified minimum essential medium (Invitrogen) supplemented with 20% FCS as described previously.[28] For induction of hematopoietic differentiation, ES cells were seeded onto a mitomycin C-treated confluent OP9 cell layer in six-well plates. Medium to support the differentiation was described elsewhere.[29] Cells at day 18 were placed in Methocult GF+ media (StemCell Technologies, Vancouver, Canada) at 1×10^4 and 1×10^5 cells per plate and clonogenic hematopoietic colonies were produced. After 14 days, individual colonies were removed and spun onto glass slides. Cells were stained with the Wright–Giemsa method. The nitro blue tetrazolium (NBT, Sigma) reduction test was performed on the cells as a granulocyte functional assay according to a previously described method.[30]

Neural differentiation

The induction of neural differentiation was carried out as described previously.[31] Day-4 embryoid bodies were plated onto tissue culture dishes and nestin-positive cells were selected in DMEM/F12 medium supplemented with 5 μg/ml of insulin (Sigma), 50 μg/ml of transferrin (Sigma), 30 nM selenium chloride (Sigma), and 5 μg/ml of fibronectin (Sigma) for 5 days. Cells were then trypsinized and plated in polyornithine-coated dishes (15 μg/ml) and expanded in N2 medium[32] supplemented with 1 μg/ml of laminin (Sigma) and 10 μg/ml of basic fibroblast growth factor (bFGF; Roche, Basel, Switzerland) for 6 days. Differentiation was induced by removal of bFGF. To confirm the neural differentiation, cells were stained with anti-human MAP-2. Briefly, cells were fixed in 4% paraformaldehyde in PBS and incubated with anti-human MAP-2 (HM-2; Sigma; diluted 1:4000) and then by Alexa Fluor 594-labeled antibody (diluted 1:500; Molecular Probe, Eugene, OR, USA). The samples were examined under a fluorescence microscope.

DNA-PCR

DNA-PCR for the SeV genome and GFP sequences was carried out as follows. DNA was extracted using the QIAamp DNA mini kits (Qiagen, Hilden, Germany) and 250 ng was used for each PCR with ExTaq (Takara, Shiga, Japan). Amplification conditions were 30 cycles of 94°C for 1 min, a variable annealing temperature (noted below) for 1 min, and 72°C for 1 min. The amplified products were run on 2% agarose gel and visualized by ethidium bromide staining. Primer sequences, annealing temperatures and product sizes were as follows: the SeV vector genome sequence: 5′-AGA GAA CAA GAC TAA GGC TAC C-3′ and 5′-ACC TTG ACA ATC CTG ATG TGG-3′ (55°C, 580 bp); the GFP sequence: 5′-CGT CCA GGA GCG CAC CAT CTT C-3′ and 5′-GGT CTT TGC TCA GGG CGG ACT-3′ (60°C, 356 bp). the cynomolgus β-actin sequence: 5′-CAT TGT CAT GGA CTC TGG CGA CGG-3′ and 5′-CAT CTC CTG CTC GAA GTC TAG GGC-3′ (60°C, 234 bp).

RNA-PCR

RNA-PCR for the SeV RNA genomic sequence was carried out as follows. Total RNA was extracted using RNA STAT-60 (Tel-Test, Friendswood, TX, USA). Reverse transcription was conducted by using Taqman reverse transcription reagents (Applied Biosystems, Foster City, CA, USA). The product (250 ng) after the reverse transcription was used for the subsequent PCR as described above.

Acknowledgements

Cynomolgus ES cells were provided by Norio Nakatsuji (Kyoto University, Kyoto, Japan), Yasushi Kondo (Tanabe Seiyaku Co. Ltd, Osaka, Japan), and Ryuzo Torii (Shiga University of Medical Science, Shiga, Japan). OP9 cells were provided by Toru Nakano (Osaka University, Osaka, Japan). We thank Yujiro Tanaka and Takayuki Asano for cultivating cynomolgus ES cells and Takeshi Hara for conducting NBT tests. We also thank Natsuko Kurosawa for technical assistance.

References

1 Thomson JA *et al.* Embryonic stem cell lines derived from human blastocysts. *Science* 1998; **282**: 1145–1147.
2 Reubinoff BE *et al.* Embryonic stem cell lines from human blastocysts: somatic differentiation *in vitro*. *Nat Biotechnol* 2000; **18**: 399–404.
3 Asano T *et al.* Highly Efficient gene transfer into primate embryonic stem cells with a simian lentivirus vector. *Mol Ther* 2002; **6**: 162–168.
4 Ma Y *et al.* High-level sustained transgene expression in human embryonic stem cells using lentiviral vectors. *Stem Cells* 2003; **21**: 111–117.
5 Gropp M *et al.* Stable genetic modification of human embryonic stem cells by lentiviral vectors. *Mol Ther* 2003; **7**: 281–287.
6 Li HO *et al.* A cytoplasmic RNA vector derived from nontransmissible Sendai virus with efficient gene transfer and expression. *J Virol* 2000; **74**: 6564–6569.
7 Yonemitsu Y *et al.* Efficient gene transfer to airway epithelium using recombinant Sendai virus. *Nat Biotechnol* 2000; **18**: 970–973.
8 Masaki I *et al.* Recombinant Sendai virus-mediated gene transfer to vasculature: a new class of efficient gene transfer vector to the vascular system. *FASEB J* 2001; **15**: 1294–1296.
9 Shiotani A *et al.* Skeletal muscle regeneration after insulin-like growth factor I gene transfer by recombinant Sendai virus vector. *Gene Therapy* 2001; **8**: 1043–1050.
10 Yamashita A *et al.* Fibroblast growth factor-2 determines severity of joint disease in adjuvant-induced arthritis in rats. *J Immunol* 2002; **168**: 450–457.

11 Ikeda Y *et al.* Recombinant Sendai virus-mediated gene transfer into adult rat retinal tissue: efficient gene transfer by brief exposure. *Exp Eye Res* 2002; **75**: 39–48.
12 Jin CH *et al.* Recombinant Sendai virus provides a highly efficient gene transfer into human cord blood-derived hematopoietic stem cells. *Gene Therapy* 2003; **10**: 272–277.
13 Crotty S *et al.* The broad-spectrum antiviral ribonucleoside ribavirin is an RNA virus mutagen. *Nat Med* 2000; **6**: 1375–1379.
14 Vo NV, Young KC, Lai MM. Mutagenic and inhibitory effects of ribavirin on hepatitis C virus RNA polymerase. *Biochemistry* 2003; **42**: 10462–10471.
15 McHutchison JG *et al.* Interferon alfa-2b alone or in combination with ribavirin as initial treatment for chronic hepatitis C. Hepatitis Interventional Therapy Group. *N Engl J Med* 1998; **339**: 1485–1492.
16 Davis GL *et al.* Interferon alfa-2b alone or in combination with ribavirin for the treatment of relapse of chronic hepatitis C. International Hepatitis Interventional Therapy Group. *N Engl J Med* 1998; **339**: 1493–1499.
17 McCormick JB *et al.* Lassa fever. Effective therapy with ribavirin. *N Engl J Med* 1986; **314**: 20–26.
18 Suemori H *et al.* Establishment of embryonic stem cell lines from cynomolgus monkey blastocysts produced by IVF or ICSI. *Dev Dyn* 2001; **222**: 273–279.
19 Spann KM, Collins PL, Teng MN. Genetic recombination during coinfection of two mutants of human respiratory syncytial virus. *J Virol* 2003; **77**: 11201–11211.
20 Tozawa H *et al.* Neutralizing activity of the antibodies against two kinds of envelope glycoproteins of Sendai virus. *Arch Virol* 1986; **91**: 145–161.
21 Tashiro M, Tobita K, Seto JT, Rott R. Comparison of protective effects of serum antibody on respiratory and systemic infection of Sendai virus in mice. *Arch Virol* 1989; **107**: 85–96.
22 Inoue M *et al.* Nontransmissible virus-like particle formation by F-deficient Sendai virus is temperature sensitive and reduced by mutations in M and HN proteins. *J Virol* 2003; **77**: 3238–3246.
23 Inoue M *et al.* A new Sendai virus vector deficient in the matrix gene does not form virus particles and shows extensive cell-to-cell spreading. *J Virol* 2003; **77**: 6419–6429.
24 Inoue M *et al.* Recombinant Sendai virus vectors deleted in both the matrix and the fusion genes: efficient gene transfer with preferable properties. *J Gene Med*, published online 5 May 2004. doi:10.1002/jgm.597.
25 Kato A *et al.* Initiation of Sendai virus multiplication from transfected cDNA or RNA with negative or positive sense. *Genes Cells* 1996; **1**: 569–579.
26 Okada T *et al.* Efficient directional cloning of recombinant adenovirus vectors using DNA–protein complex. *Nucleic Acids Res* 1998; **26**: 1947–1950.
27 Okada T *et al.* Adeno-associated viral vector-mediated gene therapy of ischemia-induced neuronal death. *Methods Enzymol* 2002; **346**: 378–393.
28 Nakano T, Kodama H, Honjo T. Generation of lympho-hematopoietic cells from embryonic stem cells in culture. *Science* 1994; **265**: 1098–1101.
29 Li F *et al.* Bone morphogenetic protein 4 induces efficient hematopoietic differentiation of rhesus monkey embryonic stem cells *in vitro*. *Blood* 2001; **98**: 335–342.
30 Sekhsaria S *et al.* Peripheral blood progenitors as a target for genetic correction of $p47^{phox}$-deficient chronic granulomatous disease. *Proc Natl Acad Sci USA* 1993; **90**: 7446–7450.
31 Lee SH *et al.* Efficient generation of midbrain and hindbrain neurons from mouse embryonic stem cells. *Nat Biotechnol* 2000; **18**: 675–679.
32 Johe KK *et al.* Single factors direct the differentiation of stem cells from the fetal and adult central nervous system. *Genes Dev* 1996; **10**: 3129–3140.
33 Takada T *et al.* Monkey embryonic stem cell lines expressing green fluorescent protein. *Cell Transplant* 2002; **11**: 631–635.

J|A|C|S
COMMUNICATIONS

Published on Web 02/24/2005

Highly Sensitive Near-Infrared Fluorescent Probes for Nitric Oxide and Their Application to Isolated Organs

Eita Sasaki,† Hirotatsu Kojima,† Hiroaki Nishimatsu,‡ Yasuteru Urano,†,§ Kazuya Kikuchi,†,§ Yasunobu Hirata,‡ and Tetsuo Nagano*,†

Graduate School of Pharmaceutical Sciences, and Faculty of Medicine, The University of Tokyo, 7-3-1 Hongo, Bunkyo-ku, Tokyo 113-0033, Japan, and PRESTO, Japan Science and Technology Corporation, Kawaguchi, Saitama, Japan

Received November 22, 2004; E-mail: tlong@mol.f.u-tokyo.ac.jp

Nitric oxide (NO), which is synthesized through conversion of L-arginine to L-citrulline by NO synthase in vivo, is an important signaling molecule involved in the regulation of a wide range of physiological and pathophysiological mechanisms, and many disorders related to NO signaling impairment have been reported.[1,2] Therefore, methods for visualizing NO would be powerful tools to examine in detail the NO signaling mechanisms[3] and might eventually be useful for diagnosis as well.

Fluorescence imaging methods are generally superior in terms of sensitivity, selectivity, and ease of use. Recently, we have successfully developed several fluorescent probes for NO,[4,5] and these probes have been widely used in biological applications. However, they have severe limitations with regard to ex vivo applications to detect NO in isolated organs since their fluorescence lies in the visible region around 500−550 nm, which cannot penetrate deeply into human tissues. While visible light is highly absorbed by biological substances, such as hemoglobin, near-infrared (NIR) light at around 650−900 nm is less absorbed by such molecules and can penetrate more deeply into tissues. Moreover, it has the further advantage that autofluorescence is not observed upon NIR excitation. For these reasons, NIR fluorescence imaging is potentially very attractive for in vivo imaging.[6] In this report, we present novel NIR fluorescent probes which are highly sensitive to NO and establish their utility by imaging NO in isolated intact rat kidneys.

The probes are composed of two moieties: tricarbocyanine as the NIR fluorophore, which has a high extinction coefficient of about $1.5-2.0 \times 10^5$ M^{-1} cm^{-1}, and *o*-phenylenediamine as the NO-sensitive fluorescence modulator. Our strategy for detecting NO is based on the change of the electron-donating ability of *o*-phenylenediamine upon selective NO-mediated transformation of diamine into triazole under aerobic conditions. We predicted that *o*-phenylenediamine should quench the fluorescence of tricarbocyanine because electron transfer should occur from *o*-phenylenediamine to the excited fluorophore. On the other hand, the corresponding triazole formation should recover its NIR fluorescence since the triazole ring should not have sufficient electron-donating ability for such photoinduced electron transfer (PeT) to occur (Scheme 1). We named these new probes diaminocyanines, DACs, and the corresponding triazole compounds DAC-Ts. They can be classified into two types; DAC-P with two propyl groups was designed to penetrate cellular membranes without any modification, and DAC-S with sulfonate groups was expected to be highly soluble in water. Consequently, the appropriate type can be selected for particular purposes.

Scheme 1

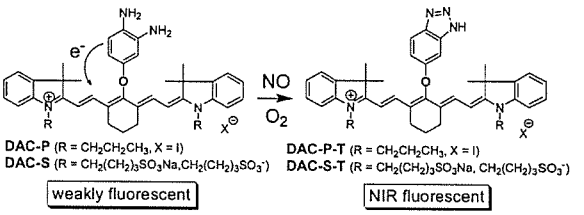

Then, we examined the spectral properties of the probes. As we expected, the NIR fluorescence intensity of DACs greatly increased in an NO concentration-dependent manner (Figure 1). The fluorescence quantum yields of DAC-Ts were 14-fold higher than that of DACs. We next evaluated the effect of pH on the fluorescence. The fluorescence of DACs was quenched at pH above 6, and that of DAC-Ts were independent of pH from 2 to 12. That is to say, DACs work well under physiological pH conditions, although the fluorescence intensities of DACs were relatively high at pH below 6. We can explain this recovery of the fluorescence under acidic conditions in terms of protonation of the amino group reducing the electron-donating ability of *o*-phenylenediamine and abolishing the PeT; the pK_a value of protonated *o*-phenylenediamine is 4.47.[7] These spectral properties indicate that PeT is successfully regulated in these molecules. According to the Rehm−Weller equation,[8] the longer the wavelength of fluorophore is, the more difficult it is for PeT to occur. As far as we know, there is only one reported NIR fluorescent probe in which the fluorescence is controlled by the PeT mechanism.[9] Therefore, it is noteworthy that we could design these fluorescent probes and control PeT in the NIR region.

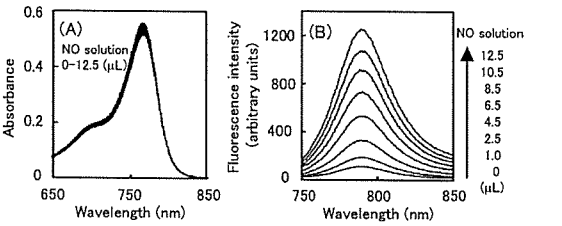

Figure 1. (A) Absorbance spectra and (B) emission spectra (excitation at 750 nm) of DAC-S (3 μM) in the presence of various amounts of NO at 37 °C in 0.1 M sodium phosphate buffer, pH 7.4. The spectra were obtained 15 min after the addition of a saturated NO aqueous solution (2 mM; 0−12.5 μL) to a solution of DAC-S (3 mL).

Furthermore, we compared the reactivity with NO of DAC-S with that of DAF-2,[4] which is a widely used NO fluorescent probe (Figure 2A). It was previously shown that the reaction rate of *o*-phenylenediamine with NO depends on electron density.[5] In the

† Graduate School of Pharmaceutical Sciences.
‡ Faculty of Medicine.
§ PRESTO.

10.1021/ja042967z CCC: $30.25

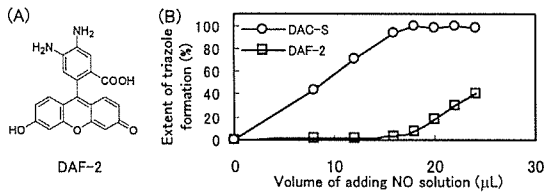

Figure 2. (A) Structure of DAF-2. (B) The extent of formation of the triazoles of DAC-S and DAF-2 (3 μM, 0.1% DMSO) after addition of various amounts of NO at 37 °C in 0.1 M sodium phosphate buffer, pH 7.4. The fluorescence intensity was measured 15 min after the addition of a saturated NO aqueous solution (2 mM; 0−24 μL) to a solution of DAC-S and DAF-2 (3 mL), and the extent of formation of the corresponding triazoles was calculated from the fluorescence quantum yields.

case of DAC-S, the electron density is increased by an electron-donating oxygen atom, while DAF-2 has an electron-withdrawing carboxylate group. Thus, DAC-S is expected to react faster than DAF-2. The result of competitive reaction of DAC-S and DAF-2 with NO is shown in Figure 2B. DAF-2 did not react with NO until almost all of the DAC-S was converted into DAC-S-T. When 8 μL of a saturated NO aqueous solution was added, 44% of DAC-S and 0.83% of DAF-2 were converted to the corresponding triazoles. Namely, the reaction efficiency of DAC-S with NO is at least 53 times higher than that of DAF-2 under an equimolar condition. This means that, although DAF-2 has functioned well in many kinds of cells so far, these new probes can potentially detect NO more effectively in biological tissues in the presence of endogenous competitors, such as thiols.

Finally, we applied DAC to isolated rat kidneys to examine whether it worked in ex vivo biological systems and whether we could observe the fluorescence change from outside the kidney without making sections. We selected DAC-P because it should be loaded more readily than DAC-S. Kidneys from male Wistar rats were isolated and perfused as described previously.[10] A diagram of the system is shown in the Supporting Information. As we expected, DAC-P was easily loaded into the kidneys simply by administering it into the right renal artery with the perfusate for several minutes and was hardly washed out throughout the observation. Then, NOC13,[11] which is an NO donor with a half-life of 4.7 min in aqueous buffer solution at pH 7.4 and 37 °C, was administered in the same manner. The NIR fluorescence images were captured every 20 s with a fluorescence stereomicroscope. We observed a fluorescence increase during the administration of NOC13 (Figure 3A). That is to say, DAC-P functions in ex vivo biological systems, and we could detect its fluorescence from outside the kidney. We noticed many circular patterns with a diameter of approximately 0.2 mm on the fluorescence images (Figure 3B−D). We confirmed that these patterns corresponded to the glomeruli inside the kidney by observing the fluorescence images of renal sections (Supporting Information). The observations are consistent with the structure of the glomeruli, which are covered with reticular blood vessels. DAC-P should be loaded into the endothelial cells during the perfusion. Thus, we succeeded in imaging NO in the isolated rat kidney using DAC-P.

In summary, we designed NIR fluorescent probes for NO, DACs, based on the PeT mechanism, synthesized them, investigated their spectral properties, compared the reaction rate with that of a widely used NO probe, DAF-2, and ascertained that they worked in isolated

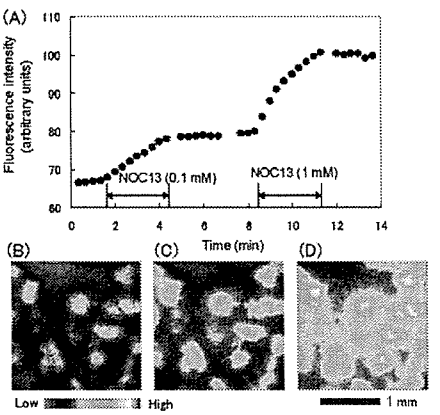

Figure 3. (A) Increase of the fluorescence intensity of DAC-P in rat kidney upon administration of NOC13. The fluorescence intensity is an averaged value calculated from an entire picture plane. The rat kidney was perfused with Krebs−Henseleit buffer at 5 mL/min. After the loading of DAC-P (5 μM) for 4 min, NOC13 (0.1 or 1 mM) was administered for 3 min (shown by arrows). (B) The captured NIR fluorescence image of a part of a rat kidney after the loading of DAC-P. (C) The image after the administration of NOC13 (0.1 mM). (D) The image after the administration of NOC13 (1 mM). All images are reproduced in pseudocolor.

rat kidneys. Because the reaction rate of DACs with NO is fast and the observation of their NIR fluorescence is less subject to interference by biological substances, our NO-detecting probes are expected to be applicable to not only cellular but also in vivo NO imaging, and work along this line is proceeding.

Acknowledgment. This work was supported in part by the Ministry of Education, Culture, Sports, Science and Technology of Japan (Grants for The Advanced and Innovational Research Program in Life Sciences to T.N., 15790070 to H.K.). H.K. was also supported by the Nissan Science Foundation, by the Nakatomi Foundation, and by the Konica Imaging Science Foundation.

Supporting Information Available: Full experimental procedures, synthesis, and characterization data for all compounds, spectral properties of DACs and DAC-Ts, pH profiles of DAC-S and DAC-S-T, a diagram of the perfused rat kidney system, and an NIR fluorescence image of a renal section. This material is available free of charge via the Internet at http://pubs.acs.org.

References

(1) Yun, H. Y.; Dawson, V. L.; Dawson, T. M. *Mol. Psychiatry* **1997**, *2*, 300−310.
(2) Napoli, C.; Ignarro, L. J. *Nitric Oxide* **2001**, *5*, 88−97.
(3) Nagano, T.; Yoshimura, T. *Chem. Rev.* **2002**, *102*, 1235−1269.
(4) Kojima, H.; Nakatsubo, N.; Kikuchi, K.; Kawahara, S.; Kirino, Y.; Nagoshi, H.; Hirata, Y.; Nagano, T. *Anal. Chem.* **1998**, *70*, 2446−2453.
(5) Gabe, Y.; Urano, Y.; Kikuchi, K.; Kojima, H.; Nagano, T. *J. Am. Chem. Soc.* **2004**, *126*, 3357−3367.
(6) Weissleder, R. *Nat. Biotechnol.* **2001**, *19*, 316−317.
(7) Dean, J. A. *Lange's Handbook of Chemistry*, 14th ed.; McGraw-Hill: New York, 1992; Section 8, 8.63.
(8) Rehm, D.; Weller, A. *Isr. J. Chem.* **1970**, *8*, 259.
(9) Ozmen, B.; Akkaya, E. U. *Tetrahedron Lett.* **2000**, *41*, 9185−9188.
(10) Kikuchi, K.; Nagano, T.; Hayakawa, H.; Hirata, Y.; Hirobe, M. *J. Biol. Chem.* **1993**, *268*, 23106−23110.
(11) Hrabie, J. A.; Klose, J. R.; Wink, D. A.; Keefer, L. K. *J. Org. Chem.* **1993**, *58*, 1472−1476.

JA042967Z

J|A|C|S
ARTICLES
Published on Web 02/19/2004

Highly Sensitive Fluorescence Probes for Nitric Oxide Based on Boron Dipyrromethene Chromophore—Rational Design of Potentially Useful Bioimaging Fluorescence Probe

Yu Gabe,† Yasuteru Urano,† Kazuya Kikuchi,†,‡ Hirotatsu Kojima,† and Tetsuo Nagano*,†

Contribution from the Graduate School of Pharmaceutical Sciences, The University of Tokyo, Hongo, Bunkyo-ku, Tokyo 113-0033, Japan, and Presto, JST Corporation, Kawaguchi, Saitama, Japan

Received August 15, 2003; E-mail: tlong@mol.f.u-tokyo.ac.jp.

Abstract: Boron dipyrromethene (BODIPY) is known to have a high quantum yield (ϕ) of fluorescence in aqueous solution but has not been utilized much for biological applications, compared to fluorescein. We developed 8-(3,4-diaminophenyl)-2,6-bis(2-carboxyethyl)-4,4-difluoro-1,3,5,7-tetramethyl-4-bora-3a,4a-diaza-*s*-indacene (DAMBO-P^{H}), based on the BODIPY chromophore, as a highly sensitive fluorescence probe for nitric oxide (NO). DAMBO-P^{H} had a low ϕ value of 0.002, whereas its triazole derivative (DAMBO-P^{H}-T), the product of the reaction of DAMBO-P^{H} with NO, fluoresced strongly (ϕ = 0.74). The change of the fluorescence intensity was found to be controlled by an intramolecular photoinduced electron transfer (PeT) mechanism. The strategy for development of DAMBO-P^{H} was as follows: (1) in order to design a highly sensitive probe of NO, the reactivity of *o*-phenylenediamine derivatives as NO-reactive moieties was examined using 4,5-diaminofluorescein (DAF-2, a widely used NO fluorescence probe), (2) in order to avoid pH-dependency of the fluorescence intensity, the PeT process was controlled by modulating the spectroscopic and electrochemical properties of BODIPY chromophores according to the Rehm−Weller equation based on measurement of excitation energies of chromophores, ground-state reduction potentials of PeT acceptors (BODIPYs), and calculation of the HOMO energy level of the PeT donor (*o*-phenylenediamine moiety) at the B3LYP/6-31G* level, (3) in order to avoid quenching of fluorescence by stacking of the probes and to obtain probes suitable for biological applications, hydrophilic functional groups were introduced. This strategy should be applicable for the rational design of other novel and potentially useful bioimaging fluorescence probes.

Introduction

In recent years, fluorescence microscopic imaging has made rapid progress as a method for monitoring biomolecules in living cells. Fluorescence probes are essential tools for biological imaging, affording high sensitivity, real-time detection, and simple measurement.[1] A large number of fluorescence probes for detecting biomolecules have been developed, but most of them were obtained not rationally but empirically. We have found that the fluorescence properties of fluorescein derivatives can be controlled by intramolecular photoinduced electron transfer (PeT),[2] and we succeeded in designing and synthesizing novel fluorescence probes based on the PeT mechanism,[3] such as DMAX for singlet oxygen.[4] If such a PeT-dependent fluorescence off/on switching mechanism is applicable to other fluorophores as well as to fluorescein derivatives, it should allow the development of novel and useful fluorescence probes for various biomolecules.

Nitric oxide (NO) plays an important role in human physiology as an intra- and extracellular messenger molecule.[5] Since NO is unstable and is produced at low concentrations, it is quite difficult to detect NO sensitively in living cells. Several years ago, we developed fluorescent indicators for NO, diaminofluoresceins (DAFs).[6] DAFs themselves are nonfluorescent but are converted to the highly fluorescent triazole forms by reaction with NO in the presence of oxygen. Among the DAFs, 4,5-diaminofluorescein (DAF-2) is widely used for real-time biological imaging of NO.[7]

* To whom correspondence should be addressed. Phone: +81-3-5841-4850. Fax: +81-3-5841-4855.
† The University of Tokyo.
‡ Presto, JST Corp.

(1) (a) Grynkiewicz, G.; Poenie, M.; Tsien, R. Y. *J. Biol. Chem.* **1985**, *260*, 3440−3450. (b) Minta, A.; Kao, J. P. Y.; Tsien, R. Y. *J. Biol. Chem.* **1989**, *264*, 8171−8178. (c) Zalewski, P. D.; Forbes, I. J.; Betts, W. H. *Biochem. J.* **1993**, *296*, 403−408.
(2) de Silva, A. P.; Gunaratne, H. Q. N.; Gunnlaugsson, T.; Huxley, A. J. M.; McCoy, C. P.; Rademacher, J. T.; Rice, T. E. *Chem. Rev.* **1997**, *97*, 1515−1566.
(3) (a) Hirano, T.; Kikuchi, K.; Urano, Y.; Higuchi, T.; Nagano, T. *J. Am. Chem. Soc.* **2000**, *122*, 12399−12400. (b) Umezawa, N.; Tanaka, K.; Urano, Y.; Kikuchi, K.; Higuchi, T.; Nagano, T. *Angew. Chem., Int. Ed. Engl.* **1999**, *38*, 2899−2901. (c) Hirano, T.; Kikuchi, K.; Urano, Y.; Higuchi, T.; Nagano, T. *Angew. Chem., Int. Ed. Engl.* **2000**, *39*, 1052−1054.
(4) Tanaka, K.; Miura, T.; Umezawa, N.; Urano, Y.; Kikuchi, K.; Higuchi, T.; Nagano, T. *J. Am. Chem. Soc.* **2001**, *123*, 2530−2536.
(5) (a) Palmer, R. M. J.; Ferrige, A. G.; Moncada, S. *Nature* **1987**, *327*, 524−526. (b) Moncada, S.; Higgs, A. *N. Engl. J. Med.* **1993**, *329*, 2002−2012. (c) Snyder, S. H.; Bredt, D. S. *Sci. Am.* **1992**, *266*, 68−77. (d) Nathan, C.; Xie, Q. *Cell* **1994**, *78*, 915−918.
(6) Kojima, H.; Nakatsubo, N.; Kikuchi, K.; Kawahara, S.; Kirino, Y.; Nagoshi, H.; Hirata, Y.; Nagano, T. *Anal. Chem.* **1998**, *70*, 2446−2453.

10.1021/ja037944j CCC: $27.50

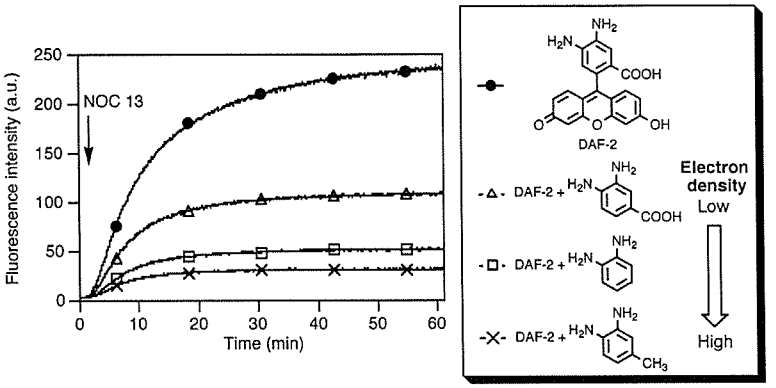

Figure 1. Inhibitory effect of *o*-phenylenediamine derivatives on the fluorescence increase in the reaction of DAF-2 with NO. The fluorescence intensity in the reaction of DAF-2 (5 μM) with NOC 13 (5 μM) was determined at 515 nm with excitation at 495 nm in the presence or in the absence of some *o*-phenylenediamine derivatives (5 μM) in 0.1 M sodium phosphate buffer (pH 7.4), containing 0.2% DMSO as a cosolvent. NOC 13 was added at the point indicated by the arrow.

However, in living cells NO is not only released at very low levels but also is lost through reactions with biomolecules such as thiols, so that there is a requirement for NO probes with higher sensitivity. More sensitive probes would need to have higher reactivity than DAF-2 with NO.

We report herein the design and synthesis of boron dipyrromethene (BODIPY)-based fluorescence NO probes that are more sensitive than DAFs. BODIPYs are of interest as chromophores due to their desirable photophysical properties.[8-10] It is also easy to modify BODIPY chemically for preparation of various derivatives. Daub et al. studied in detail the photophysical behavior of aza crown-substituted BODIPY and its analogue by means of steady-state and time-resolved fluorometry.[11] However, although fluorescein-based biological probes such as Fluo-3 (Ca^{2+} probe),[1b] DAF-2 (NO probe), and ZnAF-2 (Zn^{2+} probe)[3a] are commercially available, BODIPY-based functional probes are not yet available for biological use.

We report here the development of a pH-independent and highly sensitive fluorescence probe for NO based on the BODIPY structure.

Results and Discussion

Design of Highly Sensitive Fluorescence Probes for Nitric Oxide. DAF-2 is a commercially available NO probe, and its diester (DAF-2 DA) is useful for bioimaging of NO in living cells. First of all, we examined a way to improve DAF-2 from the viewpoint of sensitivity. The reactivity of DAFs with NO is considered to be dependent on the electron density of the *o*-phenylenediamine moiety. Figure 1 shows the degree of inhibition of the fluorescence increase due to the product (DAF-2 T) in the reaction of DAF-2 with an NO donor (NOC 13)[12] in the presence of various *o*-phenylenediamine derivatives.

Scheme 1. Reaction of DAMBO with NO

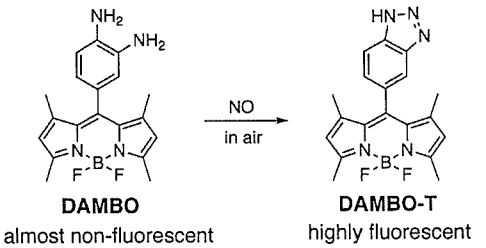

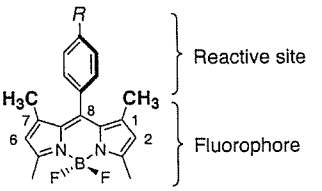

Figure 2. Structure of BODIPY with an aryl moiety. The aryl moiety (reactive site) and BODIPY (fluorophore) are twisted.

o-Phenylendiamine with electron-donating substituents caused greater inhibition of the fluorescence increase, which indicates that the reactivity toward NO is determined by the electron density of reactive sites in the *o*-phenylenediamine moiety. *o*-Phenylenediamine derivatives with high electron density are essential for improvement of the NO probe's sensitivity. DAF-2 possesses a serious disadvantage in this regard, as the *o*-phenylenediamine moiety of DAF-2 has an electron-withdrawing carboxyl functional group. However, chemical modification to remove the carboxyl functional group from the fluorescein structure of DAF-2 is impractical because 6-hydroxy-9-phenylfluorone has a low quantum yield of fluorescence (ϕ) of around 0.2.[13] Thus, a different fluorescence platform is required to design highly sensitive NO probes.

The BODIPY structure appears to be a fluorophore with potential for high sensitivity, since BODIPYs generally have high extinction coefficients and high quantum efficiencies in water as well as in organic solvents.[8] For example, 1,3,5,7-tetramethyl-8-phenyl-BODIPY is highly fluorescent.[11] It is easy to design and synthesize BODIPY-based fluorescence probes

(7) (a) Kojima, H.; Nakatsubo, N.; Kikuchi, K.; Urano, Y.; Higuchi, T.; Tanaka, J.; Kudo, Y.; Nagano, T. *Neuroreport* **1998**, *9*, 3345–3348. (b) Kuo, R. C.; Baxter, G. T.; Thompson, S. H.; Stricker, S. A.; Patton, C.; Bonaventura, J.; Epel, D. *Nature* **2000**, *406*, 633–636.
(8) Karolin, J.; Johansson, L. B.-A.; Strandberg, L.; Ny, T. *J. Am. Chem. Soc.* **1994**, *116*, 7801–7806.
(9) Kollmannsberger, M.; Gareis, T.; Heinl, S.; Breu, J.; Daub, J. *Angew. Chem., Int. Ed. Engl.* **1997**, *36*, 1333–1335.
(10) Haugland, R. P. *Handbook of Fluorescent Probes and Research Chemicals*; Molecular Probes: Eugene, OR, 2002.
(11) Kollmannsberger, M.; Rurack, K.; Resch-Genger, U.; Daub, J. *J. Phys. Chem. A* **1998**, *102*, 10211–10220.
(12) Hrabie, J. A.; Klose, J. R.; Wink, D. A.; Keefer, L. K. *J. Org. Chem.* **1993**, *58*, 1472–1476.
(13) Lindqvist, L.; Lundeen, G. W. *J. Chem. Phys.* **1966**, *44*, 1711–1712.

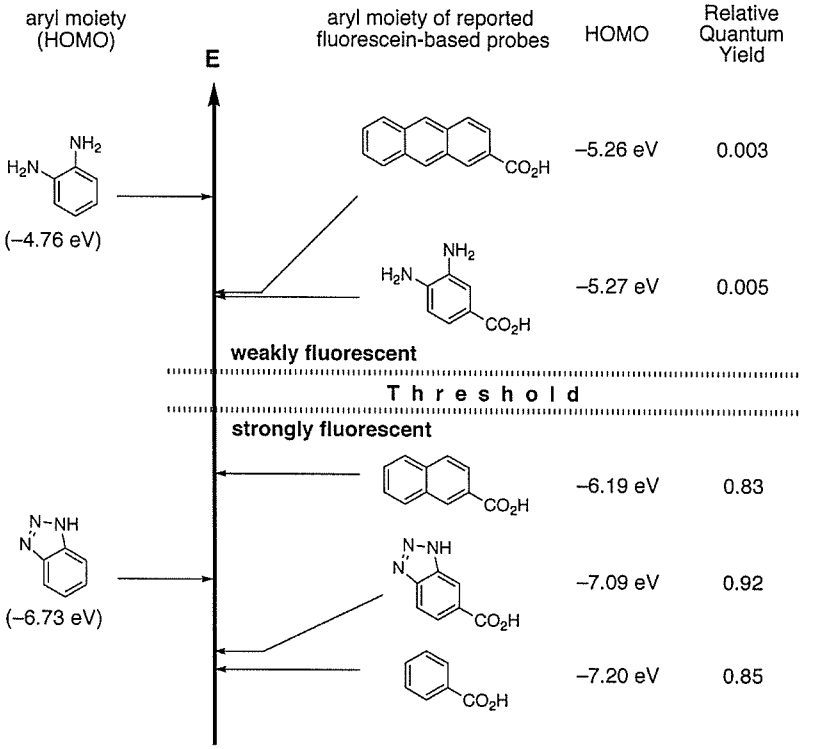

Figure 3. HOMO energy level of the aryl moiety. These values were obtained from B3LYP/6-31G* calculations.

Scheme 2. Synthetic Scheme of DAMBOs

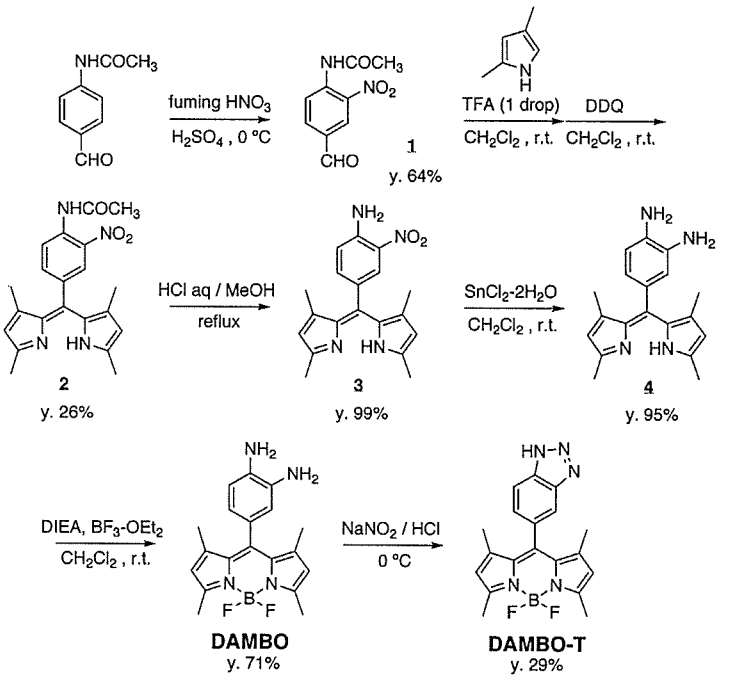

with an electron-rich reactive site for NO. In addition, derivatives of BODIPY can emit fluorescence over a wide range from 500 to 700 nm.[14] Thus, BODIPY seems to be a promising platform for sensitive fluorescence probes.

We designed a diaminobenzene-BODIPY derivative (DAMBO, Scheme 1) which does not have any electron-withdrawing functional group on *o*-phenylenediamine. Owing to the presence of the methyl groups at the C-1 and C-7 positions, the diamino-

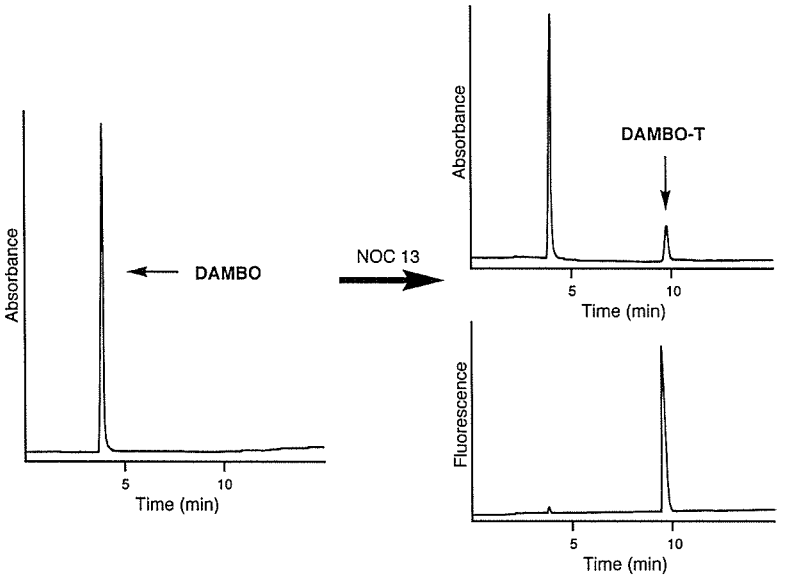

Figure 4. HPLC chromatogram in the reaction of DAMBO with NOC 13. The reaction of DAMBO (5 μM, 0.1% DMSO) with NOC 13 (20 μM) was carried out in 0.1 M sodium phosphate buffer (pH 7.4) at 37 °C for 1 h. The product was detected using HPLC: Eluent: CH_3CN/0.1% H_3PO_4 aq = 3/2; flow rate = 1.0 mL/min; detection wavelength = 495 nm (UV−Vis), 495/515 nm (fluorescence).

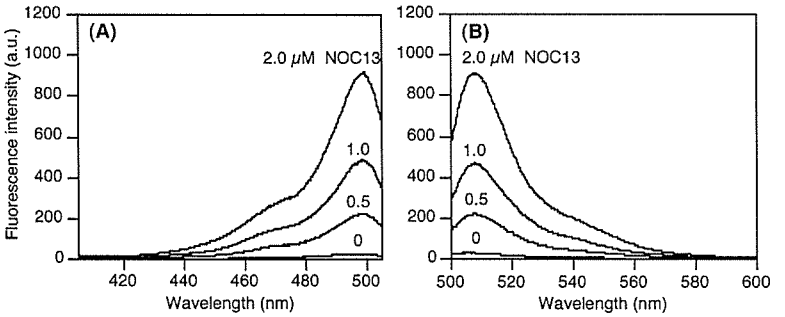

Figure 5. (A) Excitation spectra (emission at 510 nm) and (B) emission spectra (excitation at 495 nm) of DAMBO (5 μM, 0.1% DMSO) in 0.1 M sodium phosphate buffer (pH 7.4) 1 h after the reaction of various concentrations of NOC 13 ranging from 0 to 2.0 μM.

benzene moiety and BODIPY moiety are twisted and conjugatively uncoupled (Figure 2).[9] This steric structure is similar to that of fluorescein derivatives whose fluorescence properties could be controlled by the PeT mechanism. The free energy change of the PeT process can be described by the Rehm−Weller equation[15] where $E_{1/2}$ (D^+/D) and $E_{1/2}$ (A/A^-) are the

$$\Delta G_{PeT} = E_{1/2}(D^+/D) - E_{1/2}(A/A^-) - \Delta E_{00} - C$$

ground-state oxidation potential of the donor and the reduction potential of the acceptor, respectively, ΔE_{00} is the excitation energy, and C is the electrostatic interaction term.

Since the reduction potential and the excitation energy of 1,3,5,7-tetramethyl-BODIPY (BODIPY 505/515; absorbance maximum: 501 nm, reduction potential: −1.16 V vs SCE) were nearly the same as those of fluorescein,[16] the threshold of fluorescence off/on in BODIPY was expected to be similar to that in fluorescein derivatives. Thus, according to the calculation of the highest occupied molecular orbital (HOMO) energy level of the diaminobenzene moiety at the B3LYP/6-31G* level, *o*-phenylenediamine in DAMBO has a sufficiently high HOMO energy level (−4.76 eV) to make DAMBO nonfluorescent. On the other hand, triazolobenzene had a lower HOMO energy level (−6.73 eV), which suggests that DAMBO-T (triazole form), the reaction product with NO, should be highly fluorescent (Figure 3,[4] Scheme 1).

Synthesis, Fluorescence Properties, and Sensitivity of DAMBO. DAMBO was synthesized from 2,4-dimethylpyrrole and the appropriate aldehyde through four steps (Scheme 2). As expected, DAMBO reacted with NO to yield highly fluorescent DAMBO-T without any byproduct, as confirmed by HPLC (Figure 4), and the fluorescence intensity increased proportionally to the concentration of NOC 13 (Figure 5). The absorbance and fluorescence properties of DAMBO are sum-

(14) (a) Burghart, A.; Kim, H.; Welch, M. B.; Thoresen, L. H.; Reibenspies, J.; Burgess, K.; Bergström, F.; Johansson, L. B.-A. *J. Org. Chem.* **1999**, *64*, 7813−7819. (b) Chen, J.; Burghart, A.; Kovacs, A. D.; Burgess, K. *J. Org. Chem.* **2000**, *65*, 2900−2906. (c) Rurack, K.; Kollmannsberger, M.; Daub, J. *Angew. Chem., Int. Ed. Engl.* **2001**, *40*, 385−387. (d) Rurack, K.; Kollmannsberger, M.; Daub, J. *New J. Chem.* **2001**, *25*, 289−292. (e) Wada, M.; Ito, S.; Uno, H.; Murashima, T.; Ono, N.; Urano, T.; Urano, Y. *Tetrahedron Lett.* **2001**, *42*, 6711−6713.

(15) Rehm, D.; Weller, A. *Isr. J. Chem.* **1970**, *8*, 259.

(16) Miura, T.; Urano, Y.; Tanaka, K.; Nagano, T.; Ohkubo, K.; Fukuzumi, S. *J. Am. Chem. Soc.* **2003**, *125*, 8666−8671.

Table 1. Absorbance and Fluorescence Properties of DAMBOs at pH 7.4[a]

compound	absorbance max(nm)	extinction coefficient ($\times 10^4$ $M^{-1}cm^{-1}$)	emission max (nm)	relative quantum yield[b]
DAMBO	496	7.3	505	0.001
DAMBO-T	498	5.2	507	0.40
DAMBO-P^H	519	7.3	535	0.002
DAMBO-P^H-T	521	5.6	537	0.74

[a] All data were measured in 0.1 M sodium phosphate buffer (<0.2% DMSO as a cosolvent). [b] Quantum yield of fluorescence was determined using that of fluorescein (0.85) in 0.1 M NaOH aq. as a standard.

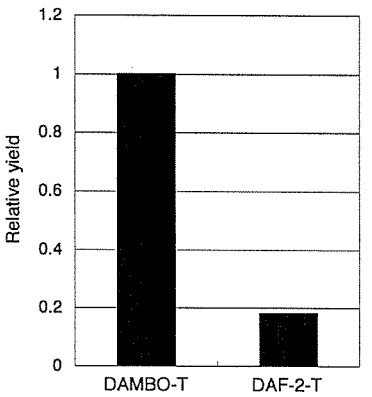

Figure 6. Relative yields of the corresponding triazoles in the competitive reaction of DAMBO and DAF-2 (5 μM, 0.1% DMSO) with NOC 13 (10 μM) in 0.1 M sodium phosphate buffer (pH 7.4). The triazoles were quantified by means of HPLC after reaction for 1 h. Eluent: CH_3CN/10 mM sodium phosphate buffer (pH 7.4) = 3/2 (DAMBOs), 6/94 (DAF-2s); flow rate = 1.0 mL/min; detection wavelength = 495 nm (UV−Vis), 495/515 nm (fluorescence).

marized in Table 1. Conversion of the diamino form to the triazole form by reaction with NO caused little change of the absorbance maxima but greatly increased the quantum efficiency, a characteristic feature of PeT probes.

Figure 6 shows a comparison of sensitivity between DAF-2 and DAMBO. In a competitive reaction, the reaction efficiency of DAMBO with NO to afford the corresponding fluorescent triazole form was about 6 times higher than that of DAF-2. These results show that raising the electron density of the reaction site is effective as a strategy to acquire higher sensitivity to NO.

Table 2. Fluorescence Increase of DAMBO after Reaction with Several ROS, Nitrite, and Nitrate[a]

reactant	after 30 min reaction	NO was added after the reaction[b]
NO[b]	280	
·OH[c]	3	250
H_2O_2[d]	2	240
NO_2^-[e]	3	270
NO_3^-[f]	2	250

[a] DAMBO (final 5 μM, 0.1% DMSO) was added to 0.1 M sodium phosphate buffer (pH 7.4). The fluorescence intensity was determined at 512 nm with excitation at 495 nm. [b] NO solution (15 μL, final 9.5 μM) was added and stirred at 37 °C for 30 min. [c] Ferrous perchlorate (100 μM) and H_2O_2 (1 mM) were added, and the mixture was stirred at 37 °C for 30 min. [d] H_2O_2 (1 mM) was added and stirred at 37 °C for 30 min. [e] $NaNO_2$ (100 μM) was added and stirred at 37 °C for 30 min. [f] $NaNO_3$ (100 μM) was added and stirred at 37 °C for 30 min.

Scheme 3. Protonated and Deprotonated Forms of DAMBO-T

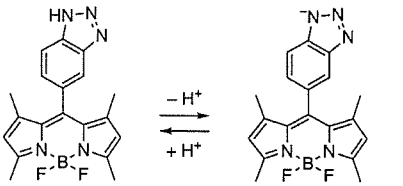

triazole form highly fluorescent **triazolate form** weakly fluorescent

Though DAMBO had higher reactivity, its selectivity for NO over various reactive oxygen species remained high. Even hydroxyl radical, the most potent oxidant among reactive oxygen species, did not generate fluorescence, and DAMBO emitted fluorescence only when reacted with NO (Table 2).

As we reported previously,[17] *o*-phenylenediamine derivatives actually react not with NO radical but with NO^+ species to yield triazole forms. Thus, probes bearing *o*-phenylenediamine derivatives as a reactive site are NO^+ probes in the strict sense. However, we consider that a fluorescence increase with our DAFs or DAMBOs at least qualitatively reflects NO production, because NO^+ species are mostly produced through very rapid oxidation of NO radical. Of course, especially in biological applications, it is desirable to use specific nitric oxide synthase inhibitors to confirm that the fluorescence increase is dependent upon the production of NO radical.

As shown in Figure 7, DAMBO could be used as a probe even in acidic aqueous media, while most fluorescein-based

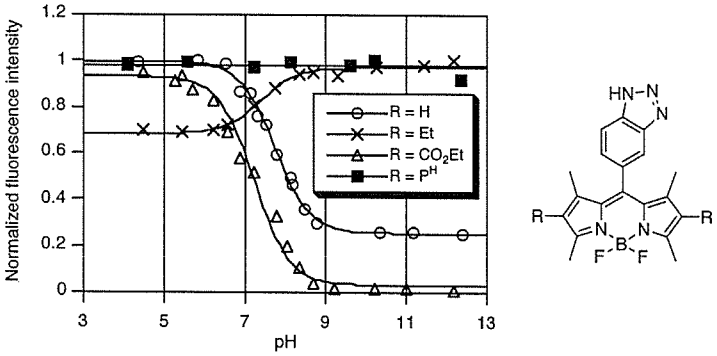

Figure 7. Effect of pH on the fluorescence intensity of DAMBO-R-Ts (R = H, P^H; 0.5 μM, 0.1% DMSO, R = Et, CO_2Et; 50 nM, 0.5% DMSO) in sodium phosphate buffer (0.1 M). The fluorescence intensities of DAMBO-T, DAMBO-Et-T, DAMBO-CO_2Et-T, and DAMBO-P^H-T were determined at 512, 535, 507, and 535 nm with excitation at 495, 520, 495, and 520 nm, respectively.

Scheme 4. Synthetic Scheme of BODIPY Derivatives

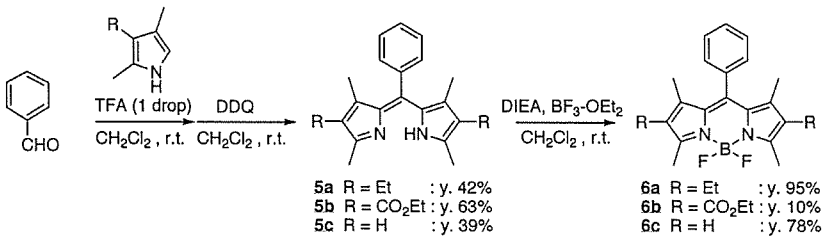

Table 3. Spectroscopic and Electrochemical Properties of BODIPY Derivatives[a]

compound	absorbance max (nm)	emission max (nm)	relative quantum yield[b]	$E_{1/2}$ (A/A$^-$) (V) vs SCE[c]	relative calcd ΔG_{PeT} (eV)[d]
6a	520	534	0.67	−1.27	+0.19
6b	496	507	0.41	−0.87	−0.33
6c	497	507	0.48	−1.19	

[a] Measured in acetonitrile (0.1% DMSO as a cosolvent). [b] Quantum yield of fluorescence was determined using that of fluorescein (0.85) in 0.1 M NaOH aq as a standard. [c] Measured in acetonitrile. Scan rate: 0.1 V s^{-1}. [d] Calculated relative ΔG_{PeT} values to that of **6c** as a standard.

probes lose fluorescence owing to lactonization reaction under acidic conditions.[18] However, Figure 7 shows that the fluorescence of DAMBO-T strikingly decreased at pH above 7. The triazolate (the deprotonated form of the triazole) of DAMBO-T was expected to be formed at pH above 7, because the pK_a value of benzotriazole is reported to be 8.27[19] and that of DAMBO-T was calculated to be 7.7 (Scheme 3). Change of fluorescence intensity around neutral pH is a serious problem and undesirable for biological imaging.

Design and Synthesis of pH-Independent NO Probe, DAMBO-P^H. The fluorescence quenching of DAMBO-T at pH above 7 can be explained by the following mechanism, i.e., the PeT process becomes accelerated because of the increased electron-donating ability of the triazolate functional group compared to the triazole functional group. The free energy change of the PeT process is determined not only by the electron-donating ability of reactive sites (benzotriazolate in this case), but also by the reduction potential and the excitation energy of the fluorophore according to the Rehm−Weller equation. Thus, to avoid the occurrence of PeT in the benzotriazolate form, we synthesized BODIPY derivatives with various substituents at the C-2 and C-6 positions to change the reduction potential and the excitation energy of the fluorophore (Scheme 4).

Introducing ethyl functional groups made the reduction potential more negative and the excitation energy smaller, while introducing ethoxycarbonyl functional groups provided the opposite results (Table 3). The fluorescence and electrochemical properties of BODIPY derivatives[9,20] were markedly changed by structural modification. The relative ΔG_{PeT} values of the two BODIPY derivatives were calculated with respect to the value for the BODIPY derivative nonsubstituted at the C-2 and C-6 positions (**6c**) as a standard. The changes of the relative ΔG_{PeT} due to the substituents at the C-2 and C-6 positions were calculated as +0.19 and −0.33 eV for **6a** and **6b**, respectively. Since the HOMO energy level of the triazolate form of DAMBO-T was located just on the threshold, the value of +0.19 eV was considered to be large enough to prevent the PeT process thermodynamically (Figure 8). In other words, the triazolate form of ethyl-substituted DAMBO-T should be highly fluorescent, while that of DAMBO-T is only weakly fluorescent.

DAMBO-T derivatives with ethyl or ethoxycarbonyl substituents at the C-2 and C-6 positions (DAMBO-R-Ts) were synthesized according to the route shown in Scheme 5. Surprisingly, the pH profiles of fluorescence of DAMBO-R-Ts show that DAMBO-Et-T was extremely fluorescent even under basic conditions (ϕ value = 0.59 at pH 7.4), independently of the pH at above 7 (Figure 7). On the contrary, the fluorescence of DAMBO-CO$_2$Et-T, with a more negative ΔG_{PeT} value, completely disappeared under basic conditions. As shown in Figure 8, benzotriazolate does not undergo an electron transfer to BODIPY with the Et functional group at R, while it does with BODIPY with the CO$_2$Et functional group at R. At pH above 7, fluorescence off/on switching could be controlled by the reaction with NO. However, there was another obstacle to the development of a novel and sensitive NO probe. The fluorescence of DAMBO-Et-T decreased slightly under acidic conditions at pH below 7, where most of DAMBO-Et-T is in the triazole form, not the triazolate form. The degree of the intensity decrease depended upon the concentration of DAMBO-Et-T (Figure 9), which suggests that the triazole form of DAMBO-Et-T was stacking in the aqueous solution, leading to the decrease of the fluorescence intensity. The BODIPY chromophore substituted with ethyl functional groups at the C-2 and C-6 positions is highly hydrophobic, while the triazolate form may not stack because of the rather hydrophilic monoanion. Thus, we designed and synthesized DAMBO-P^H with 2-carboxyethyl functional groups at the C-2 and C-6 positions (Scheme 6). Carboxyl functional groups should be effective for preventing stacking due to their higher hydrophilicity, and ethylene chains should serve to block the PeT process by changing the reduction potential and excitation energy.

The absorbance and fluorescence properties of DAMBO-P^H and DAMBO-P^H-T are shown in Table 1. The fluorescence of DAMBO-P^H-T was completely independent of pH from 3 to 13 (Figure 7), and the quantum efficiency was higher than that of DAMBO-T. Further, the Stokes shift was larger than that of DAMBO-T, which is very desirable for avoidance of light scattering and for reducing the self-absorption. Regarding sensitivity, the reaction efficiency of DAMBO-P^H with NO was higher than that of DAF-2 and the fluorescence increases of

(17) Kojima, H.; Sakurai, K.; Kikuchi, K.; Kawahara, S.; Kirino, Y.; Nagoshi, H.; Hirata, Y.; Akaike, T.; Maeda, H.; Nagano, T. *Biol. Pharm. Bull.* **1997**, *20*, 1229−1232.
(18) Chen, S.-C.; Nakamura, H.; Tamura, Z. *Chem. Pharm. Bull.* **1979**, *27*, 475−479.
(19) Wang, H.; Bruda, C.; Persy, G.; Wirz, J. *J. Am. Chem. Soc.* **2000**, *122*, 5849−5855.
(20) Kollmannsberger, M.; Rurack, K.; Resch-Genger, U.; Rettig, W.; Daub, J. *Chem. Phys. Lett.* **2000**, *329*, 363−369.